EFFECTS OF ROLLER BURNISHING ON THE SURFACE INTEGRITY AND MECHANICAL PROPERTIES OF DUPLEX AND 316L STAINLESS STEELS

A Thesis

by

Ibrahim Orhun Tugay

Submitted to the
Graduate School of Sciences and Engineering
In Partial Fulfillment of the Requirements for
the Degree of

Master of Science

in the
Department of Mechanical Engineering

Özyeğin University
January 2021

EFFECTS OF ROLLER BURNISHING ON THE SURFACE INTEGRITY AND MECHANICAL PROPERTIES OF DUPLEX AND 316L STAINLESS STEELS

Approved by:

Assoc. Prof. Dr. Güney Güven Yapıcı,
Advisor
Department of Mechanical Engineering,
Chair
Özyeğin University

Asst. Prof. Dr. Polat Şendur
Department of Mechanical Engineering
Özyeğin University

Asst. Prof. Dr. Mehmet İpekoğlu
Department of Mechanical Engineering
Turkish-German University

Date Approved: 15 January 2021

To My Family

ABSTRACT

Roller burnishing (RB) or deep rolling is a mechanical surface treatment method to enhance the surface integrity of manufactured components which affects component's performance. Although there are some valuable researches on the effects of RB on different materials, there is no comprehensive investigation about roller burnishing of duplex stainless steel (DSS) and 316L stainless steel, in a comparative manner.

The main purpose of the present thesis is to reveal the effect of RB on surface integrity and mechanical properties of duplex and 316L stainless steel. In order to understand the effect of RB parameters on surface integrity, Taguchi L9 (3^4) experimental design method was utilized. The changes in microstructure, surface microhardness, and surface roughness were measured after the RB process and the optimized parameters for the maximum surface microhardness (condition H) and the minimum surface roughness (condition R) were determined. It was shown that burnishing created a refined surface layer up to 0.6 mm and 0.8 mm, enhanced surface microhardness to 118%, and 147%, and reduced surface roughness to 52%, and 40% of the initial values, respectively for DSS and 316L.

Ambient temperature tensile tests were performed and the results revealed no notable improvement in yield and tensile strengths after the RB process. On the other hand, significant enhancements were observed in the cyclic performance after the burnishing process. Subsequently, the results of high cycle fatigue (HCF) tests revealed that the cyclic performance of the burnished sample with H condition was significantly higher than those of both unburnished and condition R samples, especially at low-stress amplitudes. Besides, fracture surface analysis exposed the restriction of

crack initiation and propagation in the hardened surface layer. Subsequently, the results of reciprocating wear tests unveiled a significant increase in wear resistance after the burnishing process. It was detected that the condition H samples have superior wear resistance in hard abrasive cases, while condition R samples are more resistive in soft abrasive conditions.

ÖZETÇE

Makaralı perdahlama işlemi, iş parçasının performansını etkileyen yüzey bütünluğünü iyileştirmek amacı ile uygulanan mekanik bir yüzey geliştirme yöntemidir. Bu konuda yapılmış değerli çalışmalar olmasına rağmen duplex ve 316L paslanmaz çeliklerinin makaralı perdahlanması ile ilgili kapsamlı bir araştırma bulumamaktadır.

Bu tez çalışmasında, makaralı perdahlama işleminin duplex ve 316L paslanmaz çeliklerinin yüzey bütünlüğü ve mekanik özellikleri üzerine olan etkisini belirlemek amaçlanmıştır. İşlemin yüzey bütünlüğü üzerindeki etkisini anlamak amacı ile Taguchi L9(3^4) deneysel tasarım metodu kullanılmıştır. Mikroyapı, yüzey sertliği ve yüzey pürüzlülğündeki değişiklikler perdahlama işleminden sonra gözlemlenmiş, maksimum yüzey mikro sertliği (koşul H) ve minimum yüzey pürüzlülüğü (koşul R) için optimize edilmiş parametreler Taguchi yöntemi ile bulunmuştur.İşlemin sırası ile duplex ve 316L paslanmaz çeliklerinde 0.6 mm ve 0.8 mm derinliğe kadar rafine olmuş bir mikroyapı oluşturduğu, 18% ve 47% yüzey mikro sertliğini arttırdığı ve 52% ve 40% yüzey pürüzlülüğünü azalttığı gözlemlenmiştir.

Ayrıca, yapılan çekme testlerinde perdahlama işlemi yapılmış malzemelerin akma ve azami çekme dayanımlarında değişiklik gözlemlenmemiştir. Bununla birlikte, perdahlama işleminin, malzemelerin yüksek çevrimli yorulma dayanımını ve aşınma performansını kayda değer miktarda arttırdığı gözlemlenmiştir.

ACKNOWLEDGEMENTS

Firstly, I am extremely grateful to my family, for their unconditional love and limitless support.

Furthermore, I would like to sincerely thank my supervisor, Dr. Güney Güven Yapıcı, for his support and guidance. I am thankful to him for his continual encouragement and assistance to carry out the current research.Also, I would like to thank our technician of the manufacturing laboratory, Mr. Ulaş Yldrm, for his contributions in this study and also my co-workers in the MEMFIS group. Especially, I would like to thank Ali Hosseinzadeh Ghobadlou for his valuable helps and suggestions.

TABLE OF CONTENTS

LIST OF TABLES

LIST OF FIGURES

CHAPTER I

INTRODUCTION

1.1 Motivation

It is well known that the mechanical performance of metallic materials is tightly related to the surface properties since mostly wear/fatigue/ corrosion-related failures start at the surface. In 1920, British scientist Griffith [1] reported that the strength of a solid body would be up to 20 times higher if the defects were eliminated. Many techniques were developed to reduce the deficiencies on the surface layer of the components.

The term which describes the surface layer quality is "surface integrity". It covers surface related parameters such as roughness, surface hardness, microstructure, and residual stress. There is a close relationship between surface integrity and functional performance of the manufactured materials. However, after machining process, surface quality of the machined components are usually diminished and defects are contained in the surface layer. To eliminate the aforementioned defects, several mechanical surface treatment (MST) methods have been developed.

MST is based on the plastic deformation of the surface of the workpiece. It is aimed to improve surface integrtiy and the mechanical properties of the materials such as fatigue life and tribological properties. Several MST techniques were utilized in the modern ages and some of them are listed below.

- Burnishing(BR)
- Shot Peening(SP)
- Laser Shock Peening (LSP)

- Ultrasonic Impact Treatment (UIT)
- Cavitation Peening (CP)
- Ultrasonic Nanocrystal Surface Modification (UNSM)

Burnishing is a chipless post-machining process to enhance the surface quality of a mechanical element. A roller made with a very high modulus material deforms the surface plastically. As a result, a mirror-like surface with higher mechanical properties are achieved. In this work, roller burnishing was applied on duplex and 316L stainless steels and the resulting properties were evaluated in a comparative manner.

1.2 Research Objectives

The present study aims to investigate the effects of roller burnishing (RB) on surface integrity and the mechanical properties (cyclic and tribological) of duplex and 316L stainless steels. The objectives were achieved through the following stages.

- Designing an effective experimental setup to determine the effect of burnishing with minimum samples.
- Investigating the influence of burnishing parameters on the surface integrity including microstructure, surface hardness, and surface roughness.
- Determining the optimized burnishing parameters to achieve the maximum surface microhardness and minimum surface roughness.
- Investigating the effects of the optimized burnishing parameters on the cyclic and tribological behavior.

1.3 Work Summary

In the present study, the roller burnishing (RB) process was used to enhance surface integrity and mechanical properties of duplex stainless steel (DSS) and 316L

stainless steel. The samples were firstly machined superficially and burnished. The optical micrographs were taken, surface roughness and microhardness of the samples were measured. A refined surface layer, enhanced surface roughness, and hardness were detected after the burnishing process. Then, the parameters were optimized to achieve the minimum surface roughness (condition R) and the maximum microhardness (condition H) by the Taguchi L9 orthogonal array. High cycle fatigue (HCF) and reciprocating wear tests were conducted on samples that were burnished with the optimized parameters. Notable enhancements were observed in the cyclic performance and tribological behavior of the burnished DSS and 316L samples.

CHAPTER II

BACKGROUND AND LITERATURE REVIEW

2.1 Hertz Contact Theory

The theoretical solution of stress distribution for two curved solid bodies in contact is based on the Hertz stress theory. It was first mentioned by Heinrich Hertz in 1882. He published the work entitled About the Contact Of Elastic Solid Bodies(ber die Berhrung FesterElasticher Korper)" in that year [2]. Hertzian contact stress refers to the localized stress that develops as two curved bodies touching each other. Firstly, Hertz, later many other researchers have contributed to the solution of elastic deformation for contacting bodies. In Hertzian calculations, it is assumed that the conditions below are met;

- The bodies are isotropic, homogeneous, obey Hooke's law, and undergo small strains and rotations
- No friction is present in the contact area
- Small amount of deformation is present compared to the principal radii of curvature of the undeformed surfaces.
- The deformations are linked to the stresses in the contact areas as foretold by the linear theory of elasticity for half-spaces (Boussinesqs control functions are valid).
- The contacting surfaces are continuous and can be described by a second-degree polynomial (quadratic surfaces) before deformation

However, the workpiece undergoes plastic deformation in burnishing process. Unfortunately, theoretical calculations of elastic-plastic stress are so difficult, even impossible because of the complexities of plastic deformation [3]. Thus, researchers use Hertz mathematical model for theoretical stress calculations. Also, it is utilized in finite modeling to predict stress distribution in burnishing [4].

The contact is between cylindrical-spherical or flat-spherical bodies for ball burnishing and cylindrical-cylindrical bodies for roller burnishing. To calculate the stresses on the bodies for burnishing the following equations (equations 1-4) are used [5].

$$a = \sqrt[3]{\frac{3F}{8}\frac{(1-\nu_1^2)/E_1(1-\nu_2^2)/E_2}{1/d_1+1/d_2}} \tag{1}$$

Where, a-contact radius, F-Force, E-Youngs Modulus, v-Poisons ratio, d-diameters of the two spheres.

Hemispherical pressure distribution, Pmax, is calculated with the following equation.

$$P_{max} = \frac{3F}{2\pi a^2} \tag{2}$$

The maximum principal stresses are calculated by the following equations(equations 3-4). The highest stress occurs on the z-axis.

$$\sigma_1 = \sigma_2 = \sigma_x = \sigma_y = -P_{max}\left[\left(\left[\frac{z}{a}\right] tan^{-1}\frac{1}{|z/a|}\right)(1+\nu) - \frac{1}{2(1+\frac{z^2}{a^2})}\right] \tag{3}$$

$$\sigma_3 = \sigma_z = \frac{-P_{max}}{1+\frac{z^2}{a^2}} \tag{4}$$

To calculate the stress on the bodies for roller burnishing process, the following equations(equations 5-9) are used.

$$a = \sqrt{\frac{2F}{\pi \iota} \frac{(1-\nu_1^2)/E_1(1-\nu_2^2)/E_2}{1/d_1 + 1/d_2}} \tag{5}$$

Where, a-half-width of rectangular contact area, l-length

Elliptical pressure distribution, Pmax, is calculated with the following equation.

$$P_{max} = \frac{2F}{\pi a \iota} \tag{6}$$

The maximum principal stresses are calculated by the following equations(equations 7-9). The highest stress occurs on the y-axis.

$$\sigma_1 = \sigma_x = -2\nu P_{max} \left(\sqrt{1 + \frac{z^2}{a^2}} - \left| \frac{z}{a} \right| \right) \tag{7}$$

$$\sigma_2 = \sigma_y = -P_{max} \left(\frac{1 + 2\frac{z^2}{a^2}}{\sqrt{1 + \frac{z^2}{a^2}}} - 2 \left| \frac{z}{a} \right| \right) \tag{8}$$

$$\sigma_3 = \sigma_z = \frac{-P_{max}}{\sqrt{1 + z^2/a^2}} \tag{9}$$

On the other hand, if the contact conditions between the surfaces violate any one of the five Hertz requirements listed above, non-Hertzian contact results. Such a contact will undoubtedly have a non-elliptical shape and non-ellipsoidal pressure distribution [6].

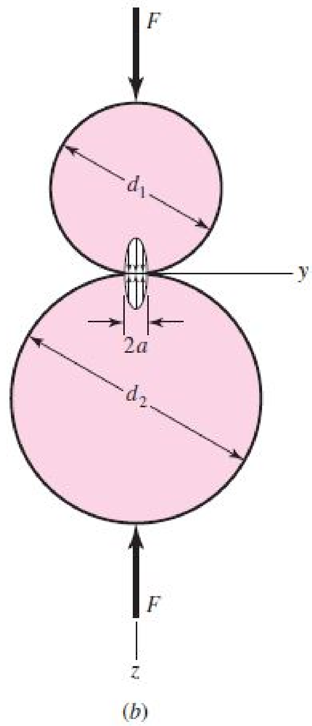

Figure 1: Contact stress distribution across the contact zone [9].

2.2 Burnishing

Surface enhancement is a common and powerful way to enhance the functional life of metals since the failures usually start on the surface. Humankind has been working to improve surface quality for thousands of years, however, systematical methods have been implemented since the first half of the 20th century [7] such as thermal, thermochemical, and mechanical techniques.

In the case of mechanical surface treatment (MST), the studies are focused on enhancing the characteristics of surface and subsurface layers of the materials after machining. Several finishing methods were developed such as shot peening, laser peening ball burnishing, and ultrasonic ball burnishing.

Burnishing is a chipless cold working process to improve the surface characteristics of the manufactured workpiece. The surface layer of the workpiece is deformed plastically by the burnishing tool to achieve the desired surface quality. It was first implemented in the US in the early 1900s and Scibner [8] patented the first burnishing tool in 1916. However, the first scientifical investigations were done in the 70s [6].

Mainly, a roller or ball made by a material with very high modulus plastically deforms the surface of the workpiece by an excessive force, which induces strain hardening. As a result, the peaks on the surface are pushed into the valleys. Plastic deformation causes dislocations in the surface layer, which induces work-hardening. One of the most beneficial outcomes of burnishing is inducing compressive residual stress beneath the surface with minimal cold work. It transforms the tensile residual stress generated from the machining process into compressive residual stress [9]. It was reported [10, 11, 3] that burnishing mitigates fatigue failure, foreign objects and wear damages and stress corrosion cracking. It can be implemented on various materials (up to 65 HRC) easily and rapidly which makes it desired for mass production. Lately, the burnishing process was employed increasingly in medical, aerospace, and nuclear industries [12]. Furthermore, Luca et al. [10] stated that burnishing is 8-15 times less expensive than grinding.

2.2.1 Physics of Burnishing

Burnishing process is a mechanical surface treatment process. In burnishing process, two physical effects can be mentioned; plastic deformation and strain or work hardening of the surface layer [13]. The peaks are lowered into the valleys due to excessive force applied by burnishing tool. As a result, the surface becomes smoother.

On the other hand, plastic deformation induces strain hardening below the surface. The strain hardening part can be divided into three parts. Firstly, stress exceeds yield strength, and the dislocation movement starts. Secondly, crystals start to rotate in the burnishing direction, which creates new dislocations in new directions. With the increase of dislocation density, dislocations are piled up, which results in a higher hardening rate. Dieter [14] stated that there are two possible dislocation mechanisms; sessile dislocation and dislocation forest. This stage is the one with the most strain hardening effect. In the third stage, some of the dislocations change the slip plane and strain hardening decreases. After each burnishing pass, the workpiece gets stronger, so the work hardening rate decreases in each extra pass [15]. Altenberger reported that roller burnishing results in the microstructures with dislocation cell structures, twinning, nanocrystallites or phase transformations [7].

Furthermore, for each burnishing technique, types of the forces that act the surface are different [13]. For ball burnishing, since the ball can rotate in all directions only normal force is present. On the other hand, for roller burnishing, the roller slides in the feed direction, thus high level of the friction force exists in the direction of feed in addition to the normal force. For slide burnishing, the tool slides in all directions since it is fully fixed. Therefore, the friction force acts in all directions.

2.2.2 Burnishing Types

Burnishing operation is similar to a machining process that can be performed in conventional-CNC lathe-milling machines. For cylindrical parts, it is similar to turning; for flat workpieces, it is similar to milling process. Both workpiece and burnishing tool are clamped in the machine as same as machining, so it is easily applicable.

According to tool type, burnishing has three main kinds; ball burnishing, roller burnishing, and slide burnishing. Also, the aforementioned types can be divided into three subdivisions according to the tip movement; ultrasonic, sonic and vibratory burnishing. Furthermore, new hybrid burnishing methods were created by combining the burnishing process with other processes. Cryogenic and laser assistant burnishing (LAB) are some of hybrid burnishing techniques.

2.2.2.1 Roller Burnishing (Deep Rolling)

In roller burnishing (RB) the burnishing tool has a roller on the tip and it is similar to the turning process. Also, it is named deep rolling in the literature. In the process, the workpiece rotates while the roller is applying force on it. The tools are classified into two groups; single roller and multi-roller tools. Also, different tools are available for internal and external applications. The roller is connected to a spring which applies the force. Roller burnishing is suitable for various cylindrical surfaces, such as grooves, bores, fillets.

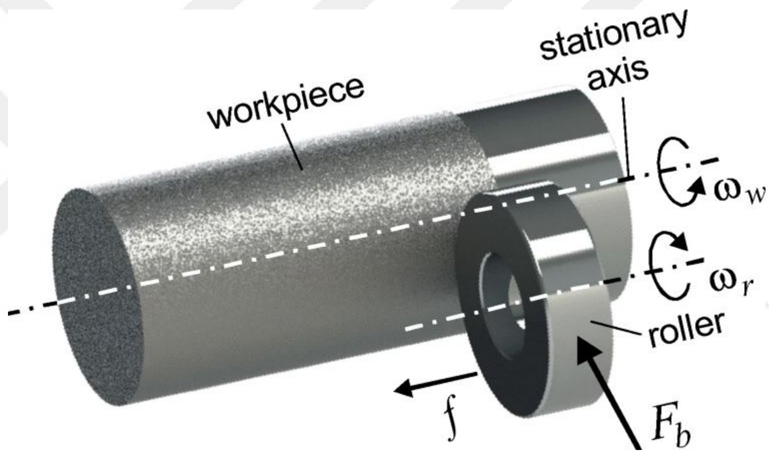

Figure 2: Representation of roller burnishing [20].

2.2.2.2 Ball Burnishing (Low Plasticity Burnishing)

In ball burnishing, the burnishing tool has a ball on the tip. Also, it is usually called as low plasticity burnishing (LPB) in the literature. Unlike roller burnishing, ball burnishing can be applied to both flat and cylindrical workpieces in the milling machine or lathe machine. The ball is hydrostatically mounted to the ball holder and rotates in all directions freely. Also, ball burnishing tools with more than one ball are available.

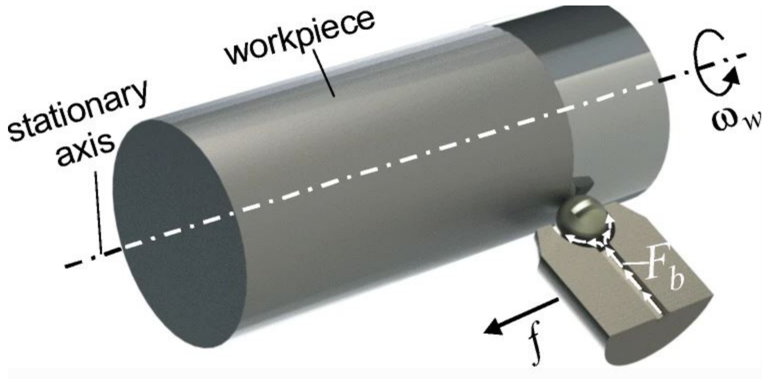

Figure 3: Representation of ball burnishing [20].

2.2.2.3 Slide Burnishing

It is similar to ball burnishing, however, in slide burnishing, the tool tip is fixed and slides purely on the workpiece. As a result of high friction during sliding, the tool wears rapidly [16]. Due to high wear, the tools are made of diamond because of its high hardness and abrasion resistance. Also, it is named as diamond or slide diamond burnishing as well. It was first implemented by General Electric in 1962 [17].

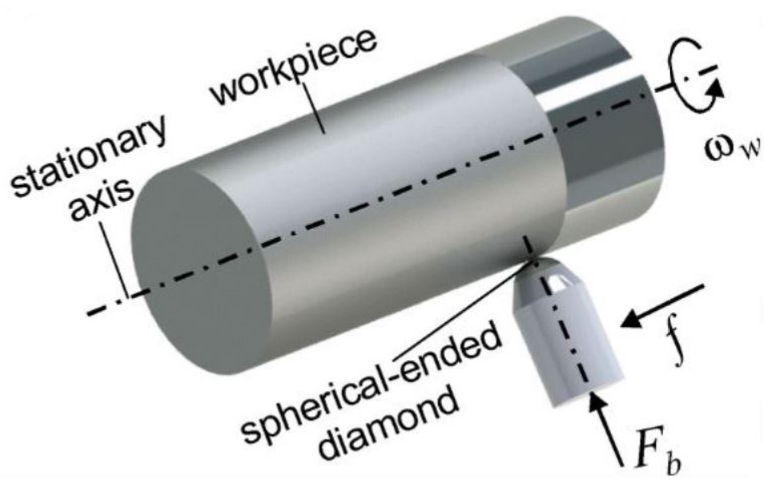

Figure 4: Representation of slide burnishing [20].

2.3 1.4462 Duplex Stainless steel

Duplex stainless steels (DSSs) are two-phased stainless steel with chromium-nickel-molybdenum-iron content. The phases contained are ferrite(δ) and austenite(γ) phases in nearly equal proportions. DSSs are classified into lean duplex, duplex, and super duplex stainless steels [18]. It was first developed in 1930 [19] and the proportions of the phases were different than now. One of the first patented duplex steel was Uranus 50 (UNS S32404) which contains 65-80% austenite . However, the modern variant was developed in 1980, which is known as 1.4462 or AISI 2205 (UNS S31803/S32205).

DSSs have superior mechanical properties. The properties are generally higher than both ferritic and austenitic steels. They have better stress corrosion cracking (SCC) resistance than austenitic steels, more toughness than ferritic steels and higher strength than both of the grades. Therefore, it can be concluded that the duplex microstructure provides high strength since it prevents grain growth, leading to a fine grain structure [20]. Furthermore, N in austenite phase solid solution hardens and increases strength. Especially, SCC resistance as one of the most important properties of duplex grade. Chromium(Cr), nitrogen(N) and molybdenum(Mo) content of DSSs gives it high corrosion resistance. Also, Cr and Mo create passive oxy-hydroxide films [20], that increases the corrosion resistance of DSSs.

2.4 316L Stainless Steel

316L stainless steel is austenitic (γ) stainless steel with chromium-nickel-molybdenum-iron content. It is a low carbon version of 316 stainless steel. L represents the low carbon content of the material. It was developed in 1950 from 316 stainless steel. The carbon content reduced to 0.03 from 0.08 to enhance the corrosion resistance of the material. Due to low carbon content, inter granular chromium carbide precipitation is less likely to occur, so, corrosion resistance is higher. Furthermore, the additional molybdenum content provides better corrosion resistance than the other austenitic steels. Also, 316L has a higher strength especially at elevated temperatures than most of the other austenitic steels such as Type 304. It can withstand up to 1300°C. 316L is a common material for medical implants, and food industry.

2.5 Surface Integrity

The expression of surface integrity refers to the surface quality of the manufactured material after the machining process. It is relatively new and it was introduced by Field and Kahles in 1964 [21]. They defined it as "the inherent or enhanced condition of a surface produced in machining or other surface generating operation". It covers the potential modifications those occur in the surface layer after manufacturing process. Grinding, honing, shot peening, and burnishing are some of the techniques those were developed to enhance surface integrity.

Researchers, who have been working on burnishing, mostly focused on the effects of burnishing parameters (force, number of passes, speed and feed, tool diameter etc.) on surface integrity [10, 22, 23]. Since temperature does not increase during burnishing, thermal effects are beside the point. Therefore, the researchers mostly focus on other aspects of surface integrity, such as residual stresses, surface roughness, and hardness.

Residual stress is an internal stress which is produced by forming process, heat treatment and/or plastic deformation. Tensile and compressive residual stresses are considered as macro stresses that exists on a multi-grain scale. Henriksen et al. [24] reported that due to the heterogeneous plastic deformation, thermal contractions, and phase transformations during machining, residual stress on the surface layer changes. It was found that normally machining process induces tensile residual stress on the surface layer [25]. Also, it remains after the machining process even temperature gradients or external forces are removed [26, 27, 28]. It is one of the most important factors in the functional life of materials, which influences fracture strength, fatigue life, corrosion resistance, and tribological properties of the workpieces [7, 29, 12, 30]. Many researchers reported that tensile residual stress lowers fatigue life and wear resistance. In contrast, compressive residual stress increases them [31].

Surface roughness is the irregularities or deviations from the nominal surface of the material in three dimensions. There is no machining operation, that produces a perfectly smooth surface. No matter how precise the operation is the surface contains irregularities and height differences that exceed interatomic distances. The flaws affect the functional life such as fatigue strength and tribological properties. Rough surface lowers fatigue life and wear resistance.

Hardness can be described as the resistance of a material against plastic deformation on the surface. It depends on the bulk properties of the material. Also, it can be increased by work hardening. Surface hardness has a vital effect on the properties of the workpiece. High surface hardness mostly means longer fatigue life and higher wear resistance.

2.6 Burnishing on Surface Integrity

Many researchers studied the influence of burnishing parameters such as feed, force, speed number of passes, tool shape, and effect of lubrication on the surface integrity. Mostly, the change of surface roughness, hardness, and residual stress were studied among the researches. All the aforesaid parameters influence surface integrity to varying levels [32]; however speed may be negligible among the others [10, 22, 33].

2.6.1 Studies on Surface Roughness

The effect of burnishing on surface roughness were studied by many researchers, and it was revealed that with the use of appropriate parameters burnishing reduces surface roughness. The final roughness depends on the burnishing parameters, the initial surface roughness, and the bulk properties of the workpiece material [10].

It was stated that burnishing is one of the most beneficial techniques to improve surface roughness among others such as grinding, and shot peening. Akkurt et al. [34] studied the effect of different hole finishing methods (drilling, turning, grinding, honing, roller burnishing, and reaming) on AISI 304 stainless steel. They found that burnishing is the best choice for high surface quality and mechanical properties. Mhaede et al. [35] compared the influence of several finishing methods (ball burnishing, conventional shot peening, ultrasound shot peening, and laser shock peening) on surface roughness of the aluminum alloy Al7075 and the titanium alloy Ti-6Al-4V. The results showed that ball burnishing is the most effective method to enhance the roughness of both the metals. Also, they noted that properties of Ti-6Al-4V improved more due to its higher bulk strength. Harish et al. [36] revealed that roller burnishing is more effective to improve the surface roughness of Al2024 than ball burnishing. Klocke et al. [37] stated that burnishing reduces surface roughness up to 50% for machined 100Cr6 steel.

Burnishing force (pressure), feed rate and the number of passes are the key factors on surface finish. Several studies revealed that roughness decreases with increasing burnishing force up to a limit force; however, excessive force results in over burnished surface and high surface roughness [38, 39]. It was suggested that force and feed are the most effective parameters on surface roughness [40]. Lacalle et al. [41] investigated burnishing on different steels and they reported that burnishing force should be proportional to the hardness of the workpiece. Excessive force results in flaws on the surface. On the other hand, Rodriguez et al. [39] stated that although the burnishing force affects the surface roughness, the effect is limited on AISI 1045 steel. Prabhu et al. [9] compared the effects of LPB and RB on AISI 4140 steel. They discovered that there is an inverse proportion between force and roughness for LPB. In contrast, in roller burnishing, they found a direct proportion between them. Furthermore, Li et al. [42] proposed an equation between burnishing force and roughness change in terms of Rz. According to the experimental results, they came up with such an equation; decrease in roughness was proportional to the square root of the burnishing force. Also, it was observed that due to hydraulic pressure loss on the tip of the tool, the actual force applied to the workpiece is less than the theoretical one for the burnishing tools working with oil [43]. Feed rate is another important factor for surface roughness, since surface roughness is closely related with tool contact geometry, especially for soft materials (20-40HRC) [13]. El-Taweel et al. [44] reported that in high feed rate, chattering occurs, which increases surface roughness. Furthermore, they noted that in high feed rate, surface heats up, which lowers surface quality. Ebeid et al. [45] stated similar results. They noted that in high feed rate the compressive effect of the tool is limited, and the surface material pushed forward, which results in a wavy surface. On the other hand, Luca [10] suggested that excessive low feed rate increases surface roughness due to extreme work-hardening. Also, Loh [32] revealed a relationship between surface roughness and feed rate by ignoring the effects of other parameters. The number of passes also affects the surface roughness. Repeating burnishing reduces roughness up to an exact limit similar to burnishing force. After the limit, roughness levels off because the hardness of the surface reaches a level that the tool can not deform it more. It was reported that [46] increasing the number of passes too much results flawing on the surface and higher surface roughness due to high work hardening. Similarly, Rao et al. [47] stated that roughness decreases with the increasing number of passes, however after four passes roughness increases on the brass workpiece. Also, they reported that ball burnishing is more effective than roller burnishing to reduce surface roughness. Furthermore, it was suggested that for hardened steels one pass is enough and more passes may give slightly better results [10]. On the other hand, for softer materials generally three or four passes are effective [48, 33].

In the case of speed, studies show that it does not have a significant effect on surface roughness [49, 50]. However, tool manufacturers suggest that it should not exceed 150 m/min. Furthermore, the use of lubricant may be the determinant factor for surface roughness. It decreases friction and temperature rise in the contact area. However, it was stated that the specification of the lubricant does not have a significant effect on surface roughness [9, 51]. In contrast, Shirsat et al. [52] showed a different result by using kerosene, 5%, and 10% graphite, SAE 30 oil, and 5%, and 10% graphite. In this study, SAE 30 oil produced slightly better surface roughness. Furthermore, Hassan et al. [51] studied the effect of different ball burnishing parameters and they revealed that large diameter balls are more efficient to decrease surface roughness.

Additionally, some researchers utilized finite element analyses (FEA) to determine the effects of burnishing on various metals. Balland et al. [53] investigated the consistency of finite element methods (FEM). They used Abaqus software and compared the results of the FEM with the experimental ones. They remarked the importance of determining the initial properties of the workpiece for precise finite element results. Bouzid et al. [54] compared experimental and FEM results of burnishing on AISI 1042 steel. They used elastic and elastic-plastic finite element models. They found the elastic-plastic model gives more accurate results than the elastic model. Similarly, John et al. [55] compared the results of experimental and computational studies. The standard deviations between the results were between 3.22 % and 8.69%.

2.6.2 Studies on Surface Hardness

The effect of burnishing on the hardness is also studied greatly, and similar outcomes were found out with the roughness case. Burnishing with the appropriate parameters enhances hardness significantly in the surface layer.

Similar to surface roughness it was suggested that burnishing is the most useful technique to improve micro-hardness. Mhaede et al. [35] analyzed the effect of ball burnishing, conventional shot peening, ultrasound shot peening, and laser shock peening on micro-hardness of the aluminum alloy Al7075 and the titanium alloy Ti-6Al-4V. The results unveiled that ball burnishing is slightly effective to enhance surface hardness of the titanium alloy. Drechsler et al. [56] investigated the effect of roller burnishing and shot peening on two different titanium alloys. They observed a harder and deeper work-hardened layer beneath the surface. Furthermore, they noted the improvement in micro-hardness closely related to the work hardening capacity of the workpiece. Sadeler et al. [57] stated that ball burnishing increases the hardness of AISI 1045 steel more than 100%. Hassan et al. [58] studied the effect of ball and roller burnishing parameters on commercial brass and aluminum. They revealed that that ball burnishing is more effective on surface hardness than roller burnishing.

Several studies suggested that an increase in the burnishing force and number of passes increases hardness [59, 60]. However, excessive force results in high strain hardening and a decrease in hardness. Also, it increases the depth of hardened layer beneath the surface. By using the Taguchi technique, the influences of burnishing parameters on hardness were investigated, and it was found that force is the most significant parameter on the hardness of the brass sample [44]. On the other hand, Revankar et al. [61] studied the effects of burnishing parameters on Ti6Al4V. The results were revealed that force has the second significant role (19.80%) on the hardness after feed rate (48.95%). Also, force must be above a limit to start plastic deformation and change the hardness. Rao et al. [47] reported that cracks developed on the surface at an excessive burnishing force. Also, they stated that ball burnishing increases hardness more than roller burnishing, even with the application of a lower force. Number of passes has similar influence on hardness with force. Hassan et. al. [58] presented that hardness increases as the increase of number of passes on aluminum and brass samples. However, after fourth pass the hardness decreases due to excessive strain hardening rate. Bourebia et al. [62] concluded that high load combined with high number of passes decreases the hardness.

In high feed-rate, the tool can not induce enough strain hardening, since the compression is limited. El-Taweel et al. [44] reported that feed-rate is the second significant parameter on hardness with an impact of 29.3%. Also, they found that spindle speed is an insignificant parameter on hardness. Tool geometry and effect of lubricant are the other parameters that were investigated less. Several studies revealed that ball burnishing is more effective in increasing hardness. Also, Prabhu et al. [9] reported that increasing ball diameter reduces the enhanecement in hardness. Hassan et al. [58] used different lubricants by various viscosities and reported no notable variation in hardness.

2.6.3 Studies on Residual Stress

Burnishing causes plastic deformation on the surface and induces compressive residual stress under the surface. It enhances mechanical properties such as cyclic and tribological properties. Several studies stated that burnishing transforms tensile residual stress resulted by machining, into compressive residual stress in the surface layer [37, 35]. Since it is related with hardness closely, variation in the parameters influences residual stress in the same manner.

Many researchers reported that burnishing induces the highest and deepest compressive residual stress among the MST techniques. Mhaede et al. [35] compared some MST methods (ball burnishing, ultrasound shot peening, shot peening, and laser peening) to improve the mechanical properties of Al7075 and Ti-6Al-4V. They revealed that ball burnishing induces the deepest and highest stress. Also, they noted that burnishing is more effective on Ti-6Al-4V than aluminum in case of inducing residual stress. Resistance to overload relaxation at high temperatures is higher for LPB compared to shot peening [46] due to minimized cold work of burnishing. Hassan et al. [63] reported a further enhancement in mechanical properties of shot peened aluminum and brass samples after burnishing.Harish et al. [36] compared the influences of roller and ball burnishing on surface integrity of Al 2024 alloy. They stated that roller burnishing induces beneficial compressive residual stress, compared to ball burnishing. Furthermore, burnishing induces a hook-shaped compressive residual stress beneath the surface [31, 64].

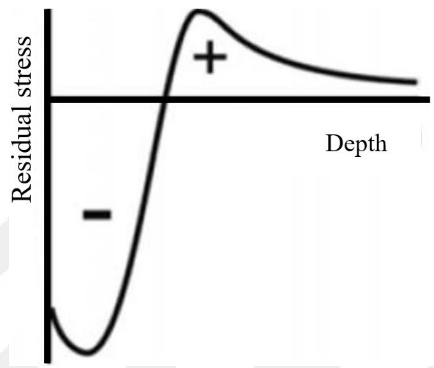

Figure 5: Representation of residual stress after burnishing process.

Many studies noted that compressive residual stress increases and deepens with the increase in burnishing force and the number of passes. Yuan et al. [65] reached the most advantageous residual stress by the highest pressure and number of passes (20 MPa-5 passes) for TA2 titanium alloy. Rodriguez et al. [39] indicated that the depth and magnitude of the stress in the axial direction increased with the higher force for AISI 1045 steel. Also, residual stress in axial direction is higher than tangential one due to burnishing directionality. The observations verified the experimental results with FE simulations. Gharbi et al. [66] reported similar results with 1050A aluminum. Salahshoor et al. [67] reported that increase in force does not affect the magnitude of residual stresses but its depth. They observed compressive residual stress up to 0.2mm depth

It was reported that low feed induces higher compressive residual stress; however, in very low feed, the surface may deteriorate. Yuan et al. [65] reported 0.2 mm/s feed for the maximum stress for TA2 titanium alloy. However, they noted the magnitude falls at lower or higher feed-rates. Similar results were reported for the effect of rotational speed. In addition, John et al. [68] developed computational and theoretical methods to calculate residual stress after burnishing and compared the results with the experimental ones for T215Cr12 tool steel. The calculated results coincided with the experimental ones. Also, it was found that smaller tool induces higher stress due to low contact area similar to hardness cases [58, 47].

2.7 Cyclic Mechanical Behavior

In the early 1800, researchers found that cracks formed inside the components exposed to fluctuating loads [69]. Finally, the part fails if the crack becomes long enough. This kind of failure known as fatigue failure. It occurs under cyclic stress even it is well below the yield strength of the material. The cracks initiate and propagate until fracture. Fatigue life is a critical aspect of engineering design, which is measured with the number of cycles until fracture.

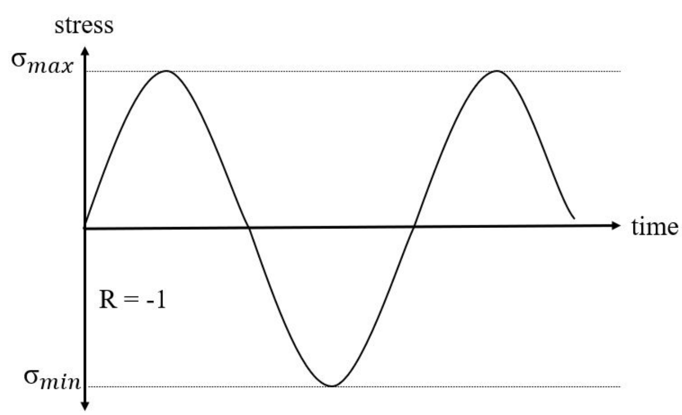

Figure 6: Schematic illustration of cyclic loading.

There are three stages of fatigue failure: crack nucleation, crack propagation, and fracture. In the first stage, the crack is nucleated where the strain is maximum [70]. In the second stage, it propagates by each cycle until fracture. In the final stage, the workpiece can not hold and it fractures fastly. Furthermore, there are two separate fatigue regimes with respect to the types of deformation that the sample experiences; low cycle fatigue (LCF) and high cycle fatigue (HCF)

LCF is characterized by plastic deformation of the sample in each cycle. Therefore, the grains deform plastically in each cycle due to high stress. A crack initiates in early cycles, and it propagates rapidly until the fracture [71]. On the other hand, HCF is characterized by elastic deformation, and initiation of the crack takes 60-90% of the life. Inhomogeneous localized plasticity initiates the crack. It may be caused by an inclusion, grain boundary or surface asperity. It can take a lot of time for a crack to cause failure. Critical crack size is one of the crucial factors for fatigue failure. Below this size the element does not fail; but, it ruptures rapidly and without any warning after the critical size [72]. Also, under a certain stress level, fatigue failure does not occur, which is known as endurance (fatigue) limit. It is supposed that the workpiece never fails below the endurance limit. However, most of the non-ferrous metals such as aluminum do not have an endurance limit [73].

The general and oldest method to treat fatigue life for HCF is plotting a stress/life (S/N) curve. Also, the curve is known as Wohler Curve since it was first used in the middle of the 1800s by August Wohler [69]. It shows the corresponding cyclic life of the component for the stress amplitude that the component undergoes. However, the curve is useful until 10^7 cycles. The stress level, which the workpiece stands until 10^7 cycles determined as the endurance limit.

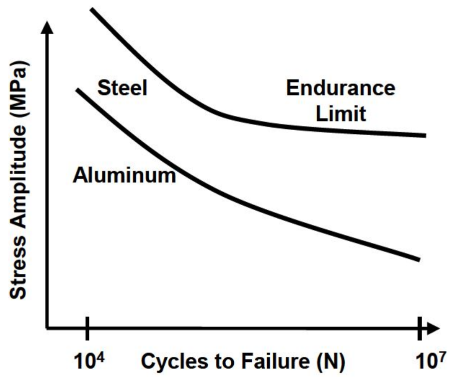

Figure 7: Illustration of a S/N curve for steel and aluminum [74].

Several factors may affect the fatigue properties of metals from intrinsic features to environmental conditions. Surface finish, microstructure, and material defects can be given as examples of the intrinsic features. To enhance the aforementioned features and fatigue properties, different MST are applied since the early ages of 20th century. For instance, in 1929 Föppl et al. [74] reported that the fatigue strength of deep-rolled thread rods were increased up to 56%. On the other hand, temperature, loading conditions, and corrosion are some of the environmental factors that affect fatigue life.

2.7.1 Effect of Burnishing on Cyclic Behavior

Several studies were performed to examine the effect of burnishing on fatigue life of different metals. It was reported that burnishing enhances fatigue life if performed by the appropriate parameters. The studies noted that compressive residual stress and good surface finish are the major factors on the fatigue life of metals [39]. On the other hand, tensile residual stress reduces fatigue life, which may be represented after machining.

It is fully understood that the compressive residual stress defines the microcrack growth rate, which influences fatigue life [59]. It is reported that compressive residual stress mitigates crack initiation and propagation phases of fatigue failure [11]. Also, it is well known that rough surface causes stress intensity on the surface which may initiate cracks. Hornbach et al. [75] reported an increase of 40% in fatigue limit and increase of fatigue life by 10x after LPB of Ti-6Al-4V. Similarly, Avils et al. [76] reported a 21.25% increase in the fatigue limit of AISI 1045 steel. Also, they noted that burnishing pushes crack initiation zone beneath the surface for low-stress cases while in high stress cracks start on the surface like the untreated samples. Prevey et al. investigated the effects of LPB extensively on aviation materials [77, 78]. They stated that burnishing improves fatigue life and foreign object damage even at high temperatures and corrosive environments. The low cold work (4-9%) decreases the relaxation rate at high temperatures and protects the compressive layer, [79, 76] as compared to shot peening.

Also, burnishing is an effective technique to increase the fatigue life of welded metals. N. Jayaraman et al. [80] studied on LPB of friction stir welded 2219-T8751 aluminum. They noted an 80% increase in fatigue life compared to the unburnished FSW aluminum. Similarly, Prevey et al. [81] reported 60% increase in the endurance limit of friction stir welded 2219-T8751 aluminum after ball burnishing process. Also, they noted that burnishing eliminated any fatigue debit from the corrosive environment. Hassanifard et al. [82] stated that high burnishing force results in a better fatigue strength for friction stir welded Al 7075T6 plates.

Furthermore, it was represented that fatigue life is correlated with the burnishing parameters. Travieso-Rodrguez et al. [83] showed that increasing burnishing force and number of passes enhance fatigue life much. Also, Sadeler et al. [57] reached similar results. Seemikeri et al. [84] suggested a high level of force, speed, and number of passes with a small ball diameter for maximizing the fatigue life of 316L stainless steel The authors related the increase in fatigue life with the increase in magnitude and depth of the work-hardened layer.

2.7.2 Tribological Behavior

Mechanical systems usually have solid parts those slide or roll against each other. Understanding the behaviors of the components in contact is the purpose of the science of tribology. The main aspects of tribology are wear and friction. The expression tribology was first used by the UK government in 1966, although many studies have been done before [85].

Wear is one of the common reasons for failure. It can be described as material removal due to microfracture, by chemical dissolution, or by melting in the contact zone. Moreover, there are numerous models of wear: abrasive, adhesive, fatigue, and corrosive. Also, in the case of contact types, there are four main types; sliding, rolling, impact, fretting, and slurry. Besides, friction is the resistance to the sliding between the contacting bodies. It has a notable impact on the mechanical systems, and despite it seems constant, it changes over time. In this thesis, the sliding contact type utilized to determine the effects of burnishing.

In abrasive wear, the stronger material damages surface of the weaker one and a groove forms. Besides, in adhesive wear the contacting materials ruptures and sticks to the mating one. Due to plastic deformation and shearing, a crack initiates, propagates towards the surface; finally, the wear particle ruptures. Fatigue and corrosive wear can be created in both elastic and plastic contacts. Fatigue wearing appears because of cyclic contact in low stress (below yielding). Due to micro defects, local yield is generated and crack initiates. In each cycle, it propagates and finally wear particle removes. When wearing takes place in a corrosive environment, reaction products are formed on the surface, which behave differently than the bulk material. This kind of wear is called corrosive wear [86]

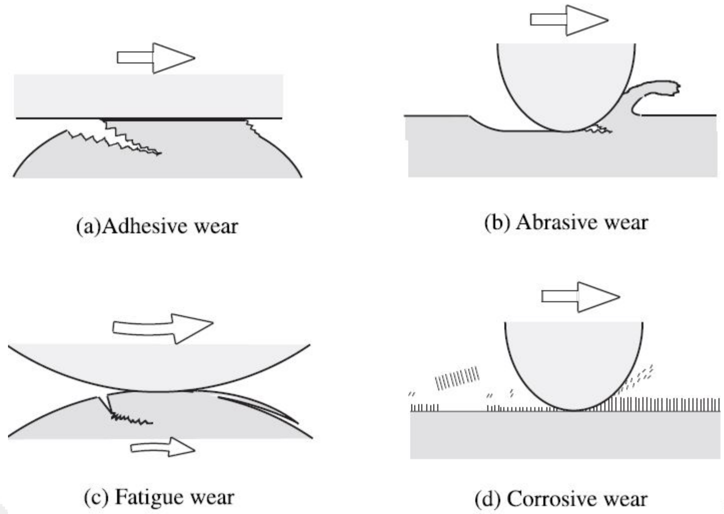

Figure 8: Schematic images of wear modes [86].

Wear-resistant steels are essential since they are the most common structural materials in all kinds of machines. Surface roughness and hardness are the critical factors for wear resistance. Low roughness increases wear resistance since asperities on the surface behave like abrasives. They cause large local stress at the contact area that damages the mating material. Moreover, wear decreases with increasing hardness if the brittle phase not introduced. Surface cracks propagate rapidly at the contact zone, and microfracture takes place in brittle steels. Additionally, work hardening, frictional heating, oxidation, and phase transformation may occur at the same time during sliding, where the importance of bulk hardness reduces. Equation 2 shows the expression that is utilized to calculate wear volume. The total volume removed "Q" is defined in equation 2.

$$Q = \frac{(K \times W)}{H} \tag{10}$$

where W is the normal load applied, which depends on contact geometry. , and K is a constant, which depends on the fraction of removed material.

2.7.3 Effect of Burnishing on Tribological Behavior

Burnishing enhances tribological properties by lowering surface roughness and increasing hardness on the surface and beneath it. A surface without asperities prevents excessive local stress that resulting from point contacts. Also, fine surfaces ensure smooth sliding and decrease friction. Improved hardness enhances wear resistance of the material. Moreover, compressive residual stress in the surface layer prevents fatigue wear by mitigating wear crack propagation.

Rajasekariah et al. [87] reported an increase in the wear resistance of steel after roller burnishing, and observed an additional increase in wear resistance in higher burnishing force. Ball burnishing increases wear resistance of brass components [88]. It was suggested that increasing burnishing force and number of passes up to a limit results in higher wear resistance. Revenkar et al. [89] suggested low feed, high burnishing force with three passes to minimize the specific wear rate of Ti6Al4V. Also, they suggested low feed, medium force, and two passes are recommended for low friction. Yilmaz et al. [90] implemented impact wear test on ball burnished 316L stainless steel. They found a dramatic decrease in volume loss after burnishing. High brittleness of the surface layer after ultrasonic burnishing deteriorates the wear performance of 7075-aluminum at high load [91]. However, at low loads burnished 7075-aluminum has higher wear resistance and lower friction.

CHAPTER III

EXPERIMENTAL SETUP

3.1 As Received Materials and Initial Preperation Details

3.1.1 1.4462 Duplex Stainless Steel (DSS)

Annealed, cold worked and polished 1.4462 duplex stainless-steel (DSS), also known as AISI 2205, rods with a diameter of 12 mm used in this study. The materials were provided by Ugitech France. The chemical composition and mechanical properties are given in Table 1 and 2, respectively.

Table 1: Chemical composition of the DSS.

Element	C	Si	Mn	Ni	Cr	Mo	S	P
wt%	0.02500	0.3530	1.5560	5.3750	22.8790	2.7810	0.0100	0.0258

Table 2: Mechanical properties of the as-received DSS.

Tensile Strength (MPa)	Yield Strength (Mpa)	Elongation (%)	Hardness (Hv)	Young's Modulus (GPa)
999	881	23	360	200

3.1.2 316L Stainless Steel

Annealed, cold worked and polished 316L, also named as AISI 1.4404, rods with a diameter of 12 mm used in this study. The materials are provided by Ugitech France. The chemical composition and mechanical properties are given in Table 3 and 4, respectively.

Table 3: Chemical composition of 316L stainless steel.

Element	C	Si	Mn	Ni	Cr	Mo	C	S
wt%	0.0130	0.4320	1.2800	10.0610	16.6330	2.0220	0.3650	0.0254

Table 4: Mechanical properties of as-received 316L stainless steel.

Tensile Strength (MPa)	Yield Strength (MPa)	Elongation (%)	Hardness (Hv)	Young's Modulus (GPa)
765	600	40	284	193

Prior to the burnishing process, all the samples were machined superficially by a CNC lathe to simulate the typical manufacturing process.

3.2 Roller Burnishing Tool

A single roller burnishing tool was used for the burnishing processes. The tool has a roller with a 40 mm diameter and made by a very high modulus material, which is attached by a spring. The tip radius of the roller is 2.5 mm to obtain the maximum work hardening with minimum plasticity. Also, an indicator was attached to the tool to arrange the force applied to the workpiece.

Figure 9: Single roller burnishing tool.

3.3 *Design of Experiment (DOE) based on the Taguchi method*

Three levels of burnishing parameters were selected by considering the compatibility to both DSS and 316L. The chosen parameters and their levels are listed in Table 5.

Table 5: Levels of burnishing parameters.

Level	Force (N)	Feed Rate (mm/rev)	Spindle Speed (rpm)	No. of Passes (n)
1	500	0.1	300	1
2	1000	0.2	600	2
3	1500	0.3	1200	3

The parameter combinations were chosen by utilizing Taguchi L9 (3^4) orthogonal array with surface roughness and surface microhardness were selected as separate response factors. The experiment parameters obtained by Taguchi technigue are illustrated in Table 6.

Table 6: Burnishing parameters.

Experiment No	Force (N)	Feed (mm/rev)	Speed (rpm)	No.of Passes
1	500	0.1	300	1
2	500	0.2	600	2
3	500	0.3	1200	3
4	1000	0.1	600	3
5	1000	0.2	1200	1
6	1000	0.3	300	2
7	1500	0.1	1200	2
8	1500	0.2	300	3
9	1500	0.3	600	1

After implementing the process with the parameters given in Table 6, surface roughness and hardness of the burnished and unburnished samples were measured. The results were analyzed by the Taguchi technique and the optimized parameters were determined for minimum surface roughness (condition R) and maximum micro-hardness (condition H), separately. For HCF and wear tests, the workpieces were burnished with the optimized parameters and the results were compared with the unburnished samples to specify the enhancement in cyclic and wear behaviors of the samples. The optimized parameters of condition H and condition R are displayed in Tables 9 and 10, respectively.

3.4 *Mechanical Testing*

3.4.1 Roughness Measurement

For the surface roughness tests D7127 ASTM standard was utilized. PCE RT-1200 handheld surface roughness meter was used for the measurements. Before the measurements, the specimens were cleaned with air and ethanol to prevent any contamination on the surface. Surface roughness in Ra was determined with a cutoff length of 0,8mm. A total of six measurements were taken for each sample from different places. The standard deviation of the results is below 6%.

3.4.2 Microhardness Measurement

For the microhardness tests E92 ASTM standard was utilized. First, the samples were ground up to 2500 grits then they were polished using the 6, 3 and 1 m diamond suspension. Future Tech FM-310 microhardness tester was used to take the measurements. Microhardness of the samples were measured using a Vickers indenter with a force of 1000 gr for 10 s. Three tests were performed in each condition to make sure about the accuracy and repeatability. The mean value of the tests were reported. The standard deviation of the results is below 5%.

3.4.3 High Cycle Fatigue Life Measurement

For fatigue testing, first, the samples were machined into the dimensions given in Figure 10 using a CNC lathe. Then, some of the specimens were burnished with the optimized burnishing parameters and the others were kept in machined conditions. Burnishing was applied to the gage section and transition radius of the specimens to ensure a homogenized stress distribution.

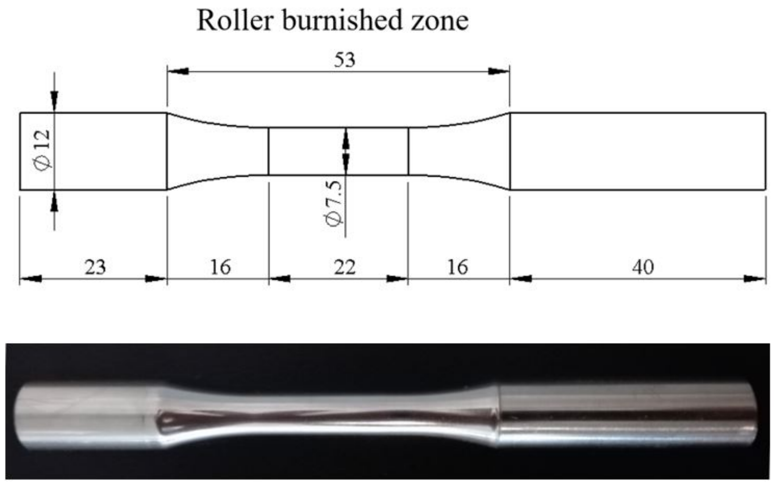

Figure 10: Illustration of the fatigue test sample.

1143 ISO standard was employed to determine the high cycle fatigue life. The specimen was mounted with a single-point bending method, and the loads were applied by dead weights hung from the free end of the specimen. The load was applied incrementally until the required value maintained without shock. The applied stress specified according to the yield stress of the materials gradually. The tests were performed at a frequency of 20 Hz at several stress ratios (Table 7) at room temperature. 10^7 cycles was accepted as the end of the test for unbroken specimens and is shown by an arrow on S/N curve indicating run-outs.

Table 7: Stress levels for the HCF tests.

Stress Level	Stress (MPa)	Stress (MPa)
	For DSS $\{\sigma_{yield} = 881MPa\}$	For 316L $\{\sigma_{yield} = 600MPa\}$
75% of σ_{yield}	679	450
80% of σ_{yield}	727	480
85% of σ_{yield}	760	510
90% of σ_{yield}	792	540
95% of σ_{yield}	840	570

3.4.4 Wear Resistance Measurement

To prepare the specimens for the wear tests, first, some of the superficially machined specimens were burnished with the optimized parameters of condition H and condition R, while the others were kept in the machined condition. Then, the specimens were cut horizontally by electrical discharge machining (EDM) with a gage length of 16 mm.

Reciprocating wear tests were employed to detect the wear resistance of the samples (Figure 11). The tests were conducted in dry condition and a high-speed steel with a Vickers hardness of 975 Hv was used as the abrasive material with a diameter of 6 mm. The tests were conducted at room temperature with the parameters of a stroke length of 10 mm and a speed of 45mm/s. A precision scale was used to measure material losses after the wear tests.

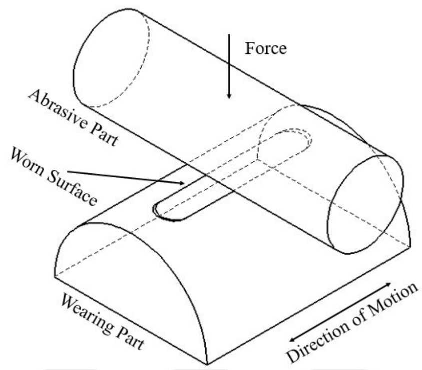

Figure 11: Illustration of wear test

To calculate the wear resistance of the samples the wear rates were calculated firstly. The wear rate and resistance of the samples were determined using equations (11) and (12).

$$WearRate = M/(F * L). \tag{11}$$

$$WearResistance = 1/(WearRate). \tag{12}$$

Three levels of normal contact forces and sliding distances were selected to analyze the effect of burnishing on the tribologic properties which are illustrated in Table 8.

Table 8: Reciprocating wear test parameters.

Levels	Contact Force, F_N (N)	Distance (m)
1	10	100
2	25	250
3	40	400

3.5 *Microstructure Evaluation methods*

3.5.1 Optical Light Microscopy

After completing the burnishing process, the samples were cut into small pieces using a micro-cutting machine. Conventional metallographic preparation procedures were employed. Grinding process using water as a lubricant to prevent damage in microstructure was made by 500, 800, 1200, 1500 and 2500 grits SiC papers. Cloths of 6, 3 and 1 m were used for polishing by a diamond suspension. Ground and polished samples were rinsed in ethanol and water after the operation to clean the particles on the surface.

For etching, different solutions were prepared for DSS and 316L. The DSS samples were electro-etched in a solution of 20 g oxalic acid and 180 ml deionized water at 3 V for 15 s. On the other hand, 316L samples were etched with Marble reagent (4 g CuSO4 in 20 ml HCl + 20 ml H2O) for 20 seconds to reveal the microstructure. Subsequently, the specimens were cleaned with water and dried. An optical microscope attached CMOS the camera was employed to reveal the grains at a magnification of 100x.

3.5.2 Scanning Electron Microscopy (SEM)

In order to observe the fracture morphology of the fractured fatigue specimens, scanning electron microscopy (SEM) was utilized with an acceleration voltage of 10 kV in a ZEISS instrument. The micrographs of the fractured fatigue samples tested in the highest and lowest stress levels were taken. In the SEM studies, it was aimed to investigate the fracture mechanisms of the specimens. Especially, effects of burnishing on crack initiation and propagation stages were studied.

CHAPTER IV

EFFECT OF BURNISHING ON THE SURFACE INTEGRITY OF DUPLEX AND 316L STAINLESS STEELS

4.1 Results and Analysis on MicroStructure

The microstructure of condition H DSS and 316L samples from the surface through the center are represented in Figures 12 and 13, respectively. A layer of refined grains with a depth of 0.9 mm was detected in the OM of condition H DSS sample (Figure 12). The grain size reduced significantly near the surface region. However, the rate of grain refinement diminishes with passing through the center of the sample. Wu et al. [92] stated that the microstructure in the aforementioned layer contains grains with intensive twins, stacking faults, and elongated sub-grains.

On the other hand, the depth of the refined layer is about 0.6 mm for condition H 316L sample (Figure 13). In this layer, although the grain boundaries became visible, the reduction of grain size is limited compared to condition H DSS sample. Furthermore, inclusions were observed near the surface of the 316L sample. Previous studies reported that the inclusions are oxides containing Mn and Si [93, 94]. Also, Song et al. [95] observed two shapes of twins in the deformed 316L samples by SEM; suspended twins and transgranular twins.

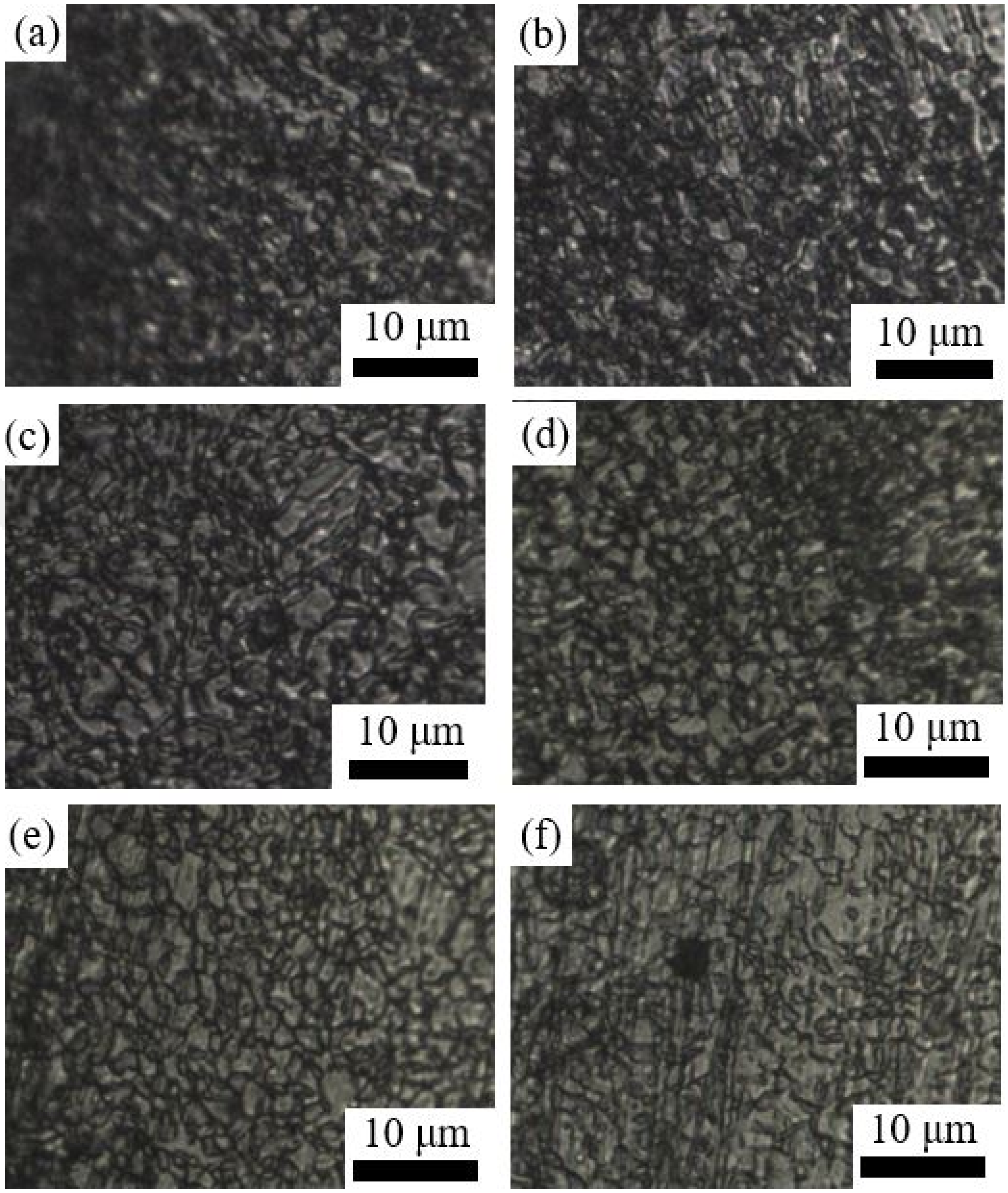

Figure 12: OM of the burnished DSS sample for the different distance of (a) 0.05 mm, (b) 0.25 mm, c) 0.45 mm, d) 0.65 mm, e) 0.85 mm, and f) 1.05 mm from the surface.

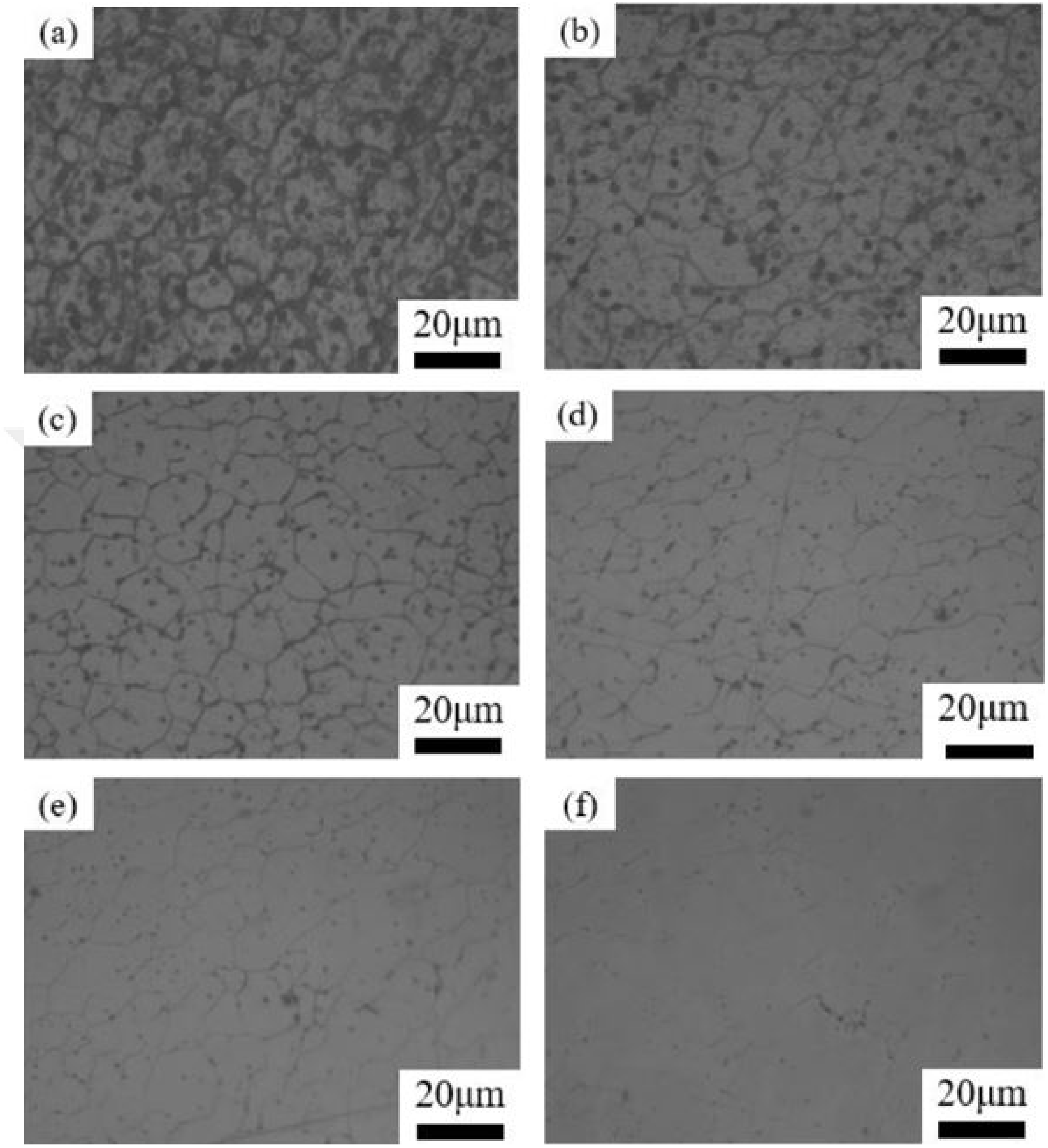

Figure 13: OM of the burnished 316L sample for the different distance of (a) 0.05 mm, (b) 0.25 mm, c) 0.45 mm, d) 0.65 mm, e) 0.85 mm, and f) 1.05 mm from the surface.

4.2 Results and Analysis on Microhardness

Figure 14 shows the surface microhardness of the samples after burnishing process. The results clearly reveals that burnishing increased surface microhardness for both DSS and 316L. However, the amount of the rise is larger for burnished 316L samples because of its weaker strength and lower initial surface microhardness compared to DSS. The maximum surface microhardness reached with Experiment 7 (Force = 1500 N, feed = 0.1 mm/rev, speed = 1200 rpm, no. of passes = 2) for both DSS and 316L. On the other hand, the minimum enhancement in surface microhardness was achieved with a force of 500N, due to low work hardening induced.

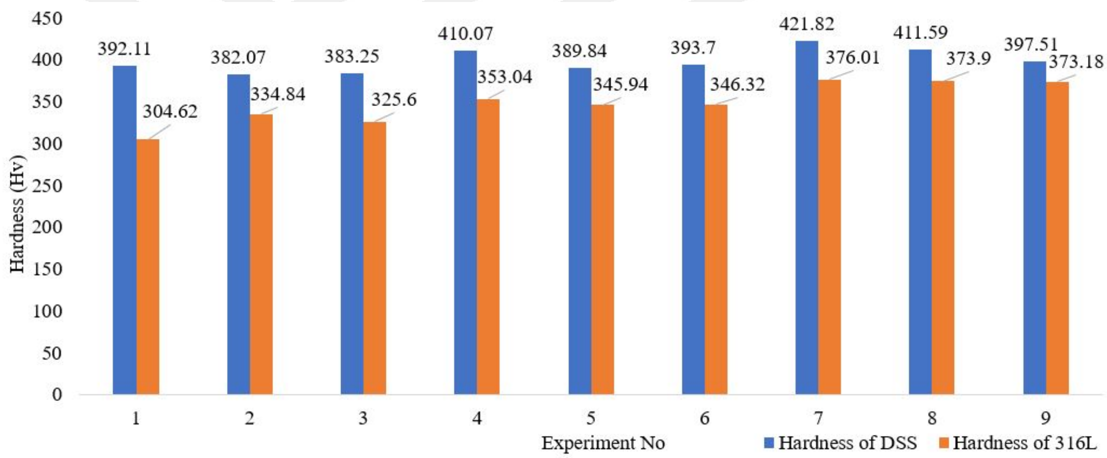

Figure 14: Surface micro hardness of the machined and burnished samples.

Figures 15 and 16 represent the effect of burnishing parameters on surface microhardness of DSS and 316L, respectively. The parameters had a similar impact on surface microhardness of DSS and 316L. It increased with rising force and the number of passes. On the other hand, increasing feed rate had a reverse effect on hardness. Besides, speed is the noneffective parameter on hardness.

The results of the Taguchi method indicated burnishing force as the most influential parameter on the surface microhardness. In the case with high burnishing force, the microhardness of the surface was enhanced significantly which can be attributed to the high work hardening rate. Similar to burnishing force, increasing the number of burnishing pass has improved the microhardness, explained by the fact that repeating burnishing enhances the structural homogeneity as well as the rate of work hardening. However, the influence of burnishing pass on the microhardness tends to decrease after each pass due to the saturation of dislocation density. Furthermore, increasing the burnishing force and the number of passes above an exact amount deteriorates the surface and consequently decreases the microhardness [96, 97]. Moreover, the increase in microhardness of 316L sample burnished with a force of 1500N is limited compared to that of the DSS sample. This phenomenon can be an attributed to work hardening capacity of 316L [98, 51].

On the other hand, surface microhardness decreased with increasing feed rate since the compressive component and work hardening rate reduces in high feed rate. Instead, the tangential component increases, and material is pushed forward. As a result, cracks were formed on the surface which reduced hardness. Besides, it was reported that in very low feed rate - high force combination, the surface deteriorates due to excessive work hardening. Additionally, the effect of speed on hardness is too low and incoherent so it may be evaluated as an insignificant parameter.

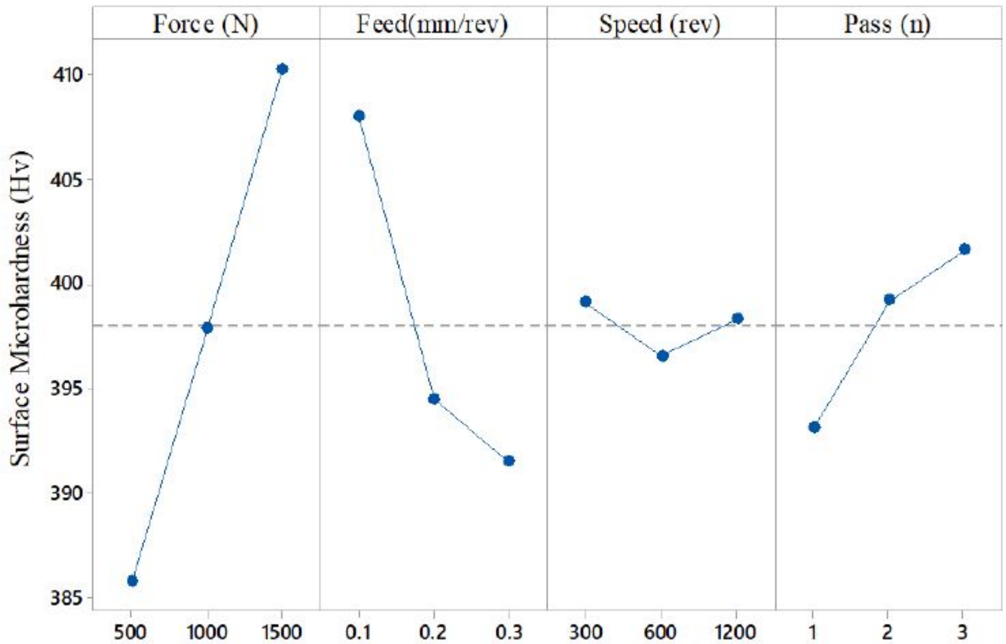

Figure 15: Effect of the burnishing parameters on surface microhardness of DSS.

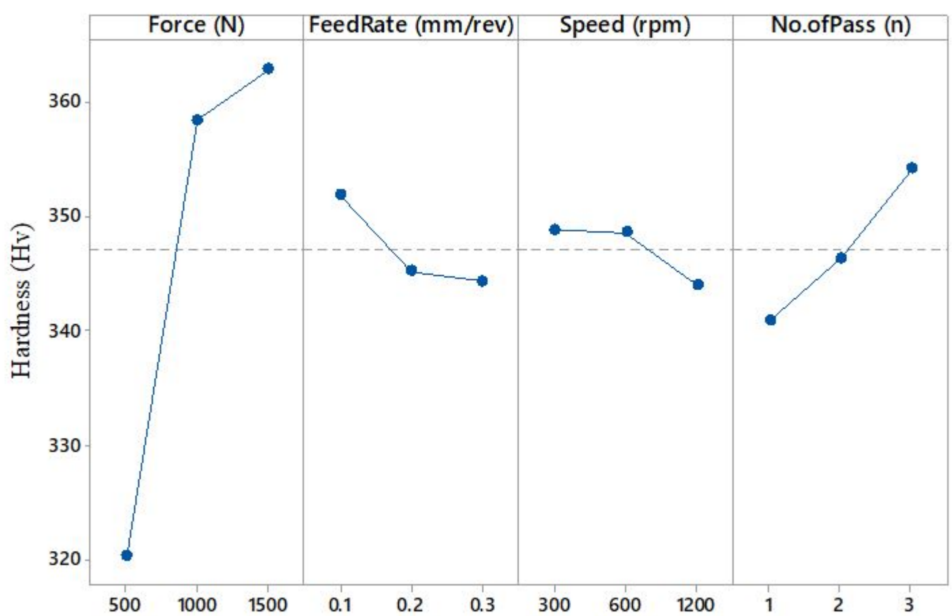

Figure 16: Effect of the burnishing parameters on surface microhardness of 316L.

According to the results of Tauchi Method, optimized burnishing parameters for the maximum surface hardness were determined. The highest hardness was reached with the same parameter combination for both DSS and 316L. The optimized parameters for maximum hardness (condition H) is represented in Table 9.

Table 9: Optimized parameters for condition H.

Parameter	Force (N)	Feed (mm/rev)	Speed (rpm)	No.of Passes
Condition H (Cond. H)	1500	0.1	300	3

Figures 17 and 18 shows the microhardness distribution in the surface layer of machined, condition H (Table 9), and condition R (Table 10) samples. Also, the figure is useful to understand residual stress distribution in this layer. The depth of the work-hardened layer is about 0.9 mm for condition H and approximately 0.4 mm for condition R 316L, while it is about 0.8 mm for condition H and approximately 0.6 mm for condition R DSS. For condition H 316L sample, low microhardness on the surface may be linked with surface deterioration [23]. Also, a similar phenomenon was observed for condition R 316L sample. Besides, for machined 316L sample, low microhardness between the surface and a depth of 0.2 mm may be attributed to tensile residual stress induced by machining operation.

On the other hand, microhardness decreased gently up to 0.8mm beneath the surface for condition H DSS sample and maximum microhardness was observed on the surface. Nevertheless, the hardened layer was observed up to 0.5mm beneath the surface for condition R DSS.

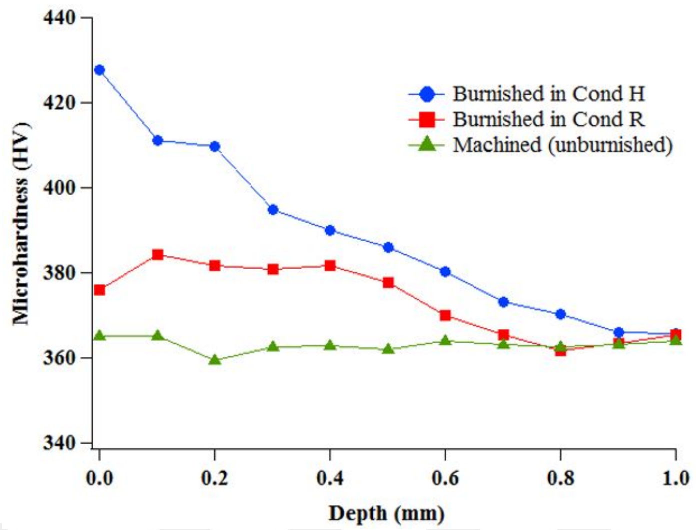

Figure 17: Microhardness distribution beneath the surface for unburnished, condition R and condition H DSSs.

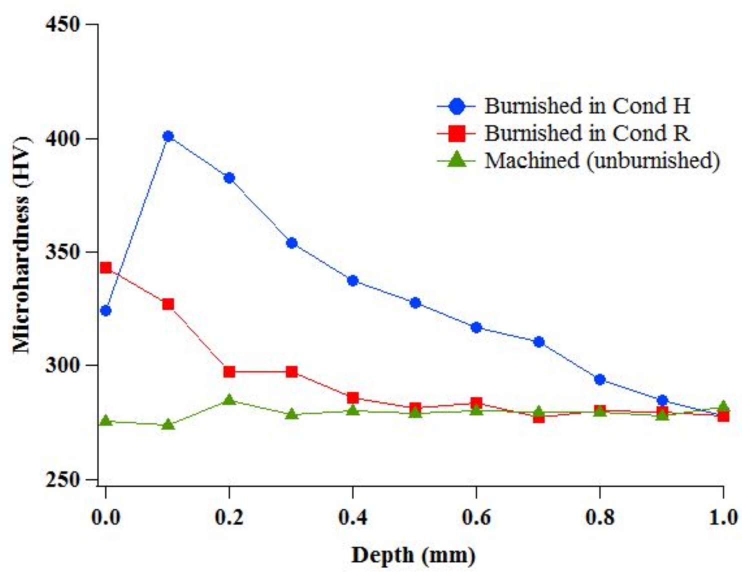

Figure 18: Microhardness distribution beneath the surface for unburnished, condition R and condition H 316Ls.

Moreover, the agreement of relation between the microhardness and average grain size of the condition H samples with Hall-Petch is depicted in Figures 19 and 20, respectively for DSS and 316L. For 316L, hardness on the surface was neglected due to surface deterioration. The Hall-Petch relationship is given by

$$H = H_0 + k_h d^{-0.5} \tag{13}$$

where H is the microhardness in HV, and d is the average grain size at different interval distances from the surface of the burnished sample. Also, H_o is the microhardness intercept at $d^{-0.5} = 0$ and k_h is the slope of the $H - d^{-0.5}$curve [99]. The figures reveal that the relation between the microhardness and average grain size of the condition H sample is well interpreted with the Hall-Petch relation. Microhardness of the sample increased with decreasing the grain size.

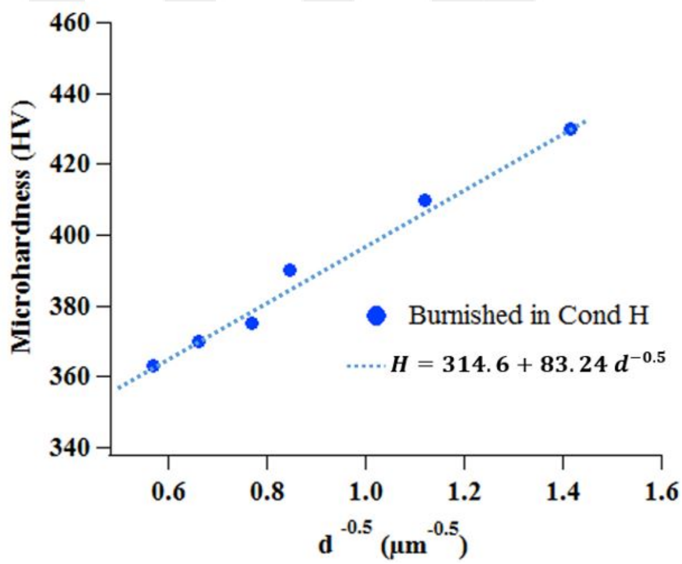

Figure 19: Microhardness as a function of grain size for DSS describing the Hall-Petch equation.

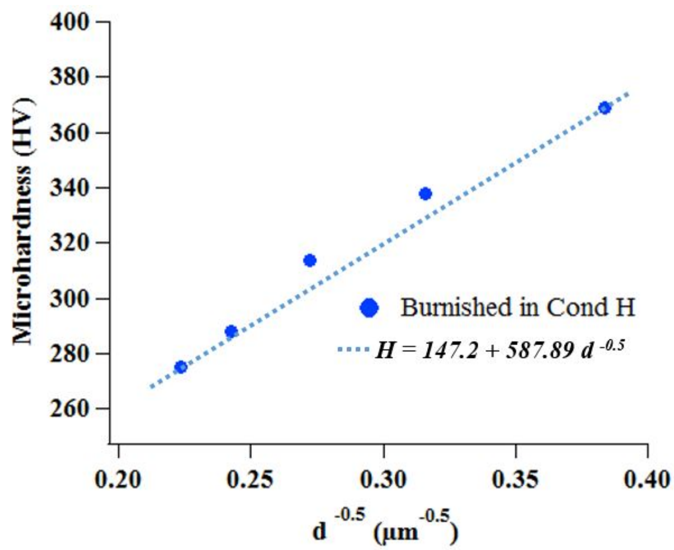

Figure 20: Microhardness as a function of grain size for 316L describing the Hall-Petch equation.

4.3 Results and Analysis on Surface Roughness

Figure 21 shows the surface roughness of machined and burnished samples. It is clearly demonstrated that burnishing with the appropriate parameters reduced surface roughness significantly. Also, although burnishing parameters have similar effects on the surface roughness for both materials, burnishing decreased surface roughness of DSS more. This phenomenon may be explained by the higher bulk hardness of DSS. For decreasing surface roughness of 316L more, a lower burnishing force may be required. The smoothest surface was achieved with Parameter 4 (Force = 1000N, feed = 0.1 mm/rev, speed = 600rpm, number of passes = 3); while the roughest surface was obtained with the Parameter 9 (Force = 1500 N, feed = 0.3 mm/rev, speed = 600 rpm, number of passes = 1).

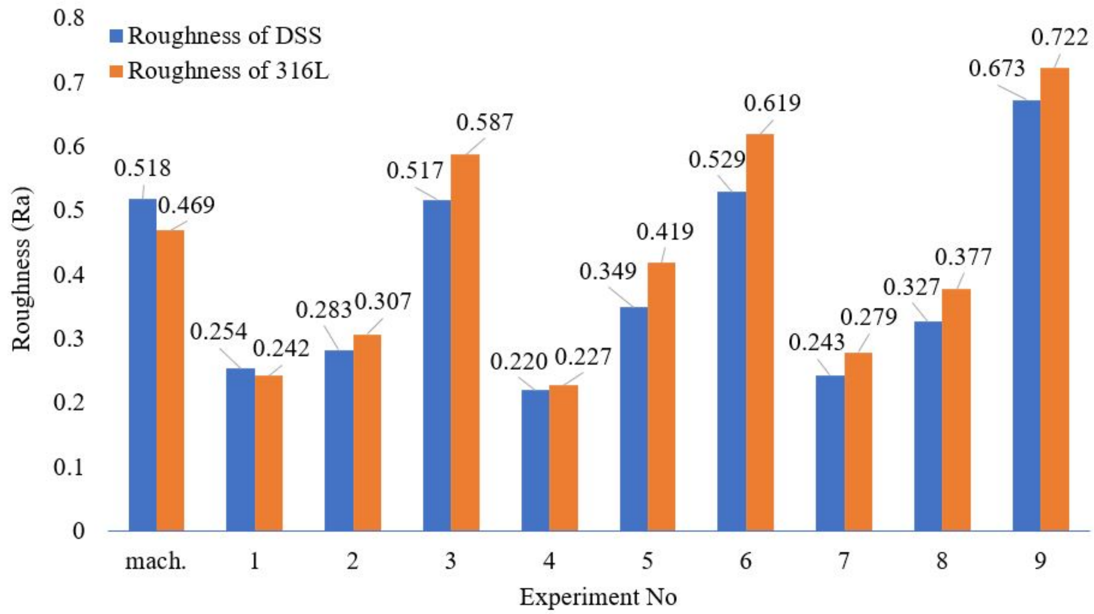

Figure 21: Surface roughness of the machined and burnished samples.

Figures 22 and 23 demonstrate the influence of the parameters on the surface roughness, respectively for DSS and 316L. It is seen that surface roughness increased with rising force and feed rate, while it reduced with the increasing number of passes. However, as it is obvious from the results of the Taguchi method rotational speed does not have a notable effect on surface roughness.

As illustrated in Figures 21 and 22, the feed rate is the most important parameter which significantly affects the surface roughness of the samples throughout the burnishing process. At high feed rates, the surface material is pushed forward intensively which results in a wavy surface. Also, it was indicated that the high feed rate causes chattering on the surface [51]. In contrast, at very low feeds, due to excessive work hardening, the surface is deteriorated [9, 65].

Besides, a rise in the force increases surface roughness. Although the threshold amount of force must be exceeded to start plastic deformation, excessive force deteriorates the surface [48]. It was reported that excessive force produces a wavy surface by pushing the material upward [100] or pilling it up in front of the roller [101]. On the other hand, it was stated that too low burnishing force can not deform surface thus, does not reduce surface roughness[101, 45, 43]. Furthermore, it is seen that surface roughness of 316L was more sensitive to high burnishing force due to it's lower strength.

As shown in Figures 22 and 23, although the surface roughness reduced after two burnishing passes, there was not a significant change in roughness for the third pass. This stability of surface roughness can be attributed to the enhanced microhardness of the burnished sample. Moreover, it was reported by Loh et al. [32] increasing the number of passes too much results in flawing on the surface and consequently higher surface roughness. Furthermore, unless the smoothest surface obtained at the lowest speed (300rpm), the effect of speed is too low and can be considered as an ineffective parameter within certain limits which is well agreed with the results of El-Taweel [45] for burnishing of AlZnMg aluminum alloy.

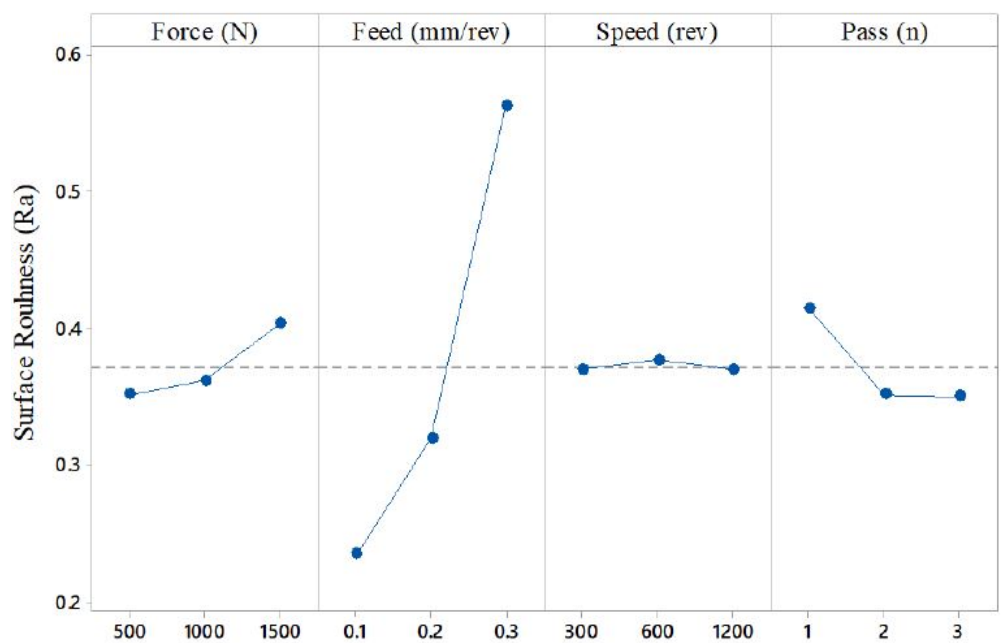

Figure 22: Effect of the burnishing parameters on surface roughness of DSS.

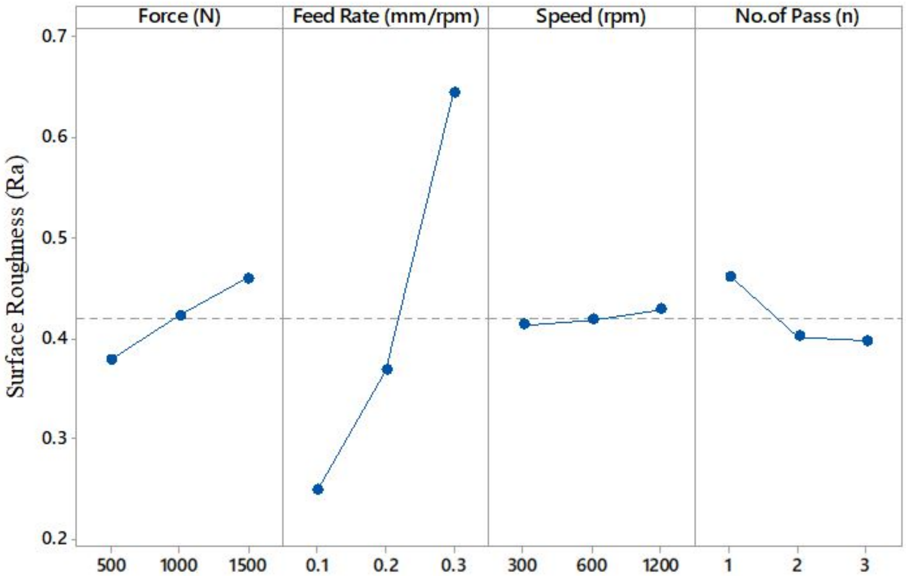

Figure 23: Effect of the burnishing parameters on surface roughness of 316L.

The optimized parameters for surface roughness is illustrated in Table 10 found via Taguchi method. The lowest surface roughness reached with the same parameters for both DSS and 316L.

Table 10: Optimized parameters for condition R.

Parameter	Force (N)	Feed (mm/rev)	Speed (rpm)	No.of Passes
Condition R (Cond. R)	500	0.1	300	3

Figure 24 shows the surface roughness of Condition R and Condition H burnished samples. Although high roughness of machined DSS sample, the burnished DSS samples have lower surface roughness than that of 316L samples. The surface roughness decreased about 50% for 316L and 60% for DSS compared to machined conditions. Also, burnishing with the condition H parameter (Table 9) reduced the surface roughness compared to the machined samples. Surface roughness reduced approximately

20% for316L and a 35% for DSS after burnishing with condition H parameter. The low reduction rate of 316L samples can be attributed to lower bulk strength and hardness of 316L.

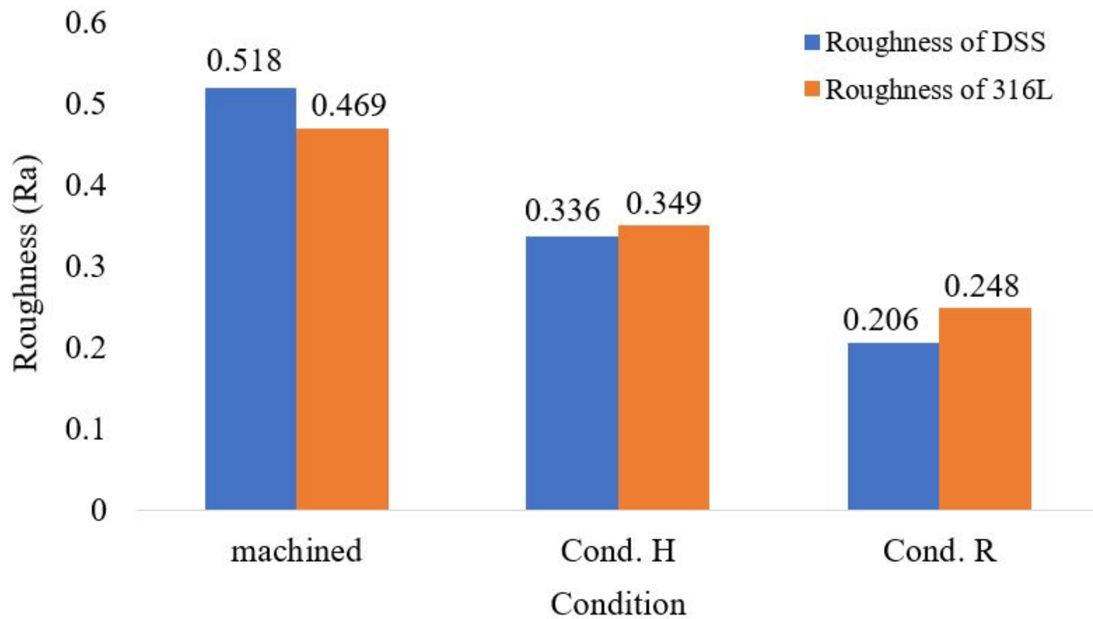

Figure 24: Surface roughness of machined, condition H and condition R samples.

CHAPTER V

EFFECT OF BURNISHING ON THE FATIGUE LIFE AND WEAR BEHAVIOR OF DUPLEX STAINLESS STEELS

5.1 Results and Analysis of Monotonic Mechanical Behaviour

Figures 25a and b illustrate stress-strain curves of unburnished and condition H DSS samples, respectively. Tensile strength rose about 3% and yield strength increased approximately 1% after the burnishing process. Tensile strengths are 999 Mpa and 1031 MPa and yield strengths are 881 MPa and 893 MPa, respectively for unburnished and condition H samples. As burnishing only affects a thin layer beneath the surface of the samples, the tensile properties of their full sections remain practically unchanged so the improvement in tensile properties is relatively low. Gharbi et al. [102]stated the limited enhancement in the strength may be attributed to work hardened surface and low roughness. On the other hand, percent elongation at fracture was 47.49% and 43.87%, respectively for unburnished and condition H DSS samples.

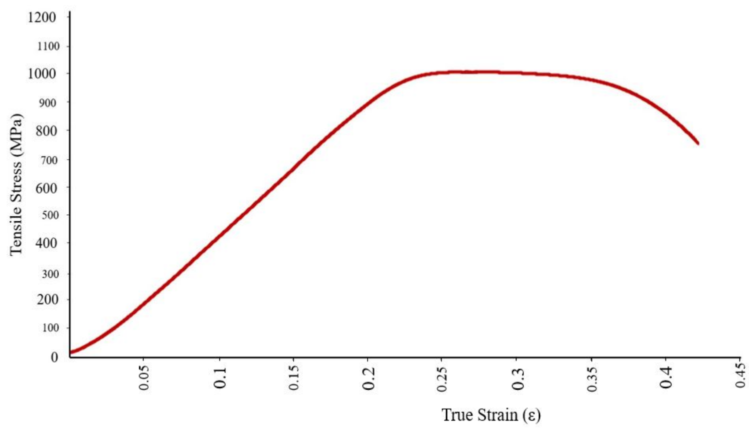

(a)

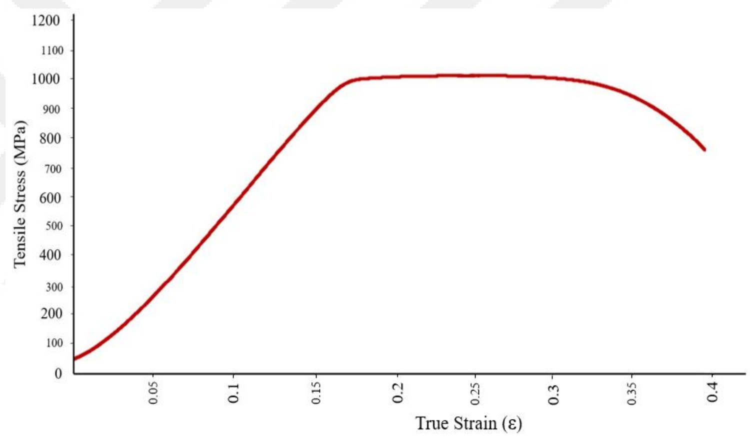

(b)

Figure 25: Stress-Strain curves of a)Unburnished DSS, b) Condition H DSS.

5.2 Results and Analysis on HCF Life

Figure 26 demonstrates the results of HCF tests of DSS samples on a semi-log scale and the arrow indicates run out. It is obvious that burnishing enhanced the fatigue strength of DSS for both optimized parameters of condition H and condition R. The main reason for this enhancement is compressive residual stress induced by the burnishing process, which restricts the initiation and propagation of fatigue cracks [103].

Inspection of data gathered from the S-N curve was revealed that the difference between the fatigue lives of the burnished and unburnished samples is more significant at low stress amplitudes. This can be attributed to the relaxation of residual stress at high fatigue stresses amplitudes [104]. Comparing the fatigue performance of condition H and condition R, the fatigue lives of the condition H samples were higher than that of condition R samples which may be linked with the higher induced compressive residual stress[105].

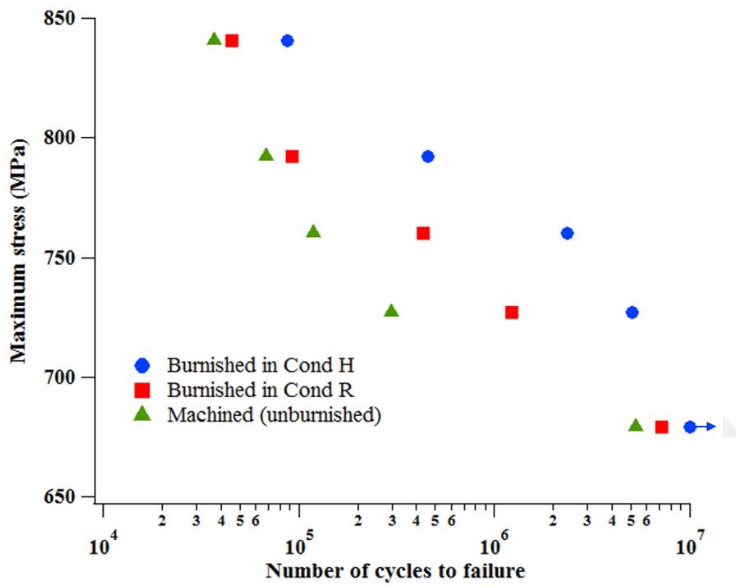

Figure 26: HCF results of the unburnished, condition R and condition H DSS samples (arrow indicates run out)

Additionally, the lower surface roughness of burnished samples increases fatigue life by reducing the high stress concentration zones on the surface. It was stated in the previous studies the smooth surface decreases the amount of the regions with high crack initiation potential [106, 103].

5.3 Fracture Morphology Analysis

Figures 27-38 represent the fracture surfaces of the DSS samples tested at high and low stress amplitudes, respectively. A crenelated shape was observed on the fracture surface of the unburnished DSS sample tested at high stress amplitude (Figure 27) due to multiple crack progression lines. Several cracks initiated on the surface due to rough surface and high stress amplitude. The turning marks caused localized stress concentration on the surface and as the test advanced, the cracks propagated through the center until the fast fracture. Similar behavior was reported by Klotz et al. [107], who described that the turning marks on the surface have an initiator effect in the formation of fatigue cracks. An example of the fatigue cracks observed on the surface is shown in Figure 28.

On the other hand, less amount of cracks were observed on the fracture surface of the unburnished sample tested in low stress amplitude (Figure 29). However, parallel two crack progressions, which initiated on the surface, were caused fatigue failure of the sample (Figure 30). The cracks propagated through the center of the sample until the resistant segment reduced to the critical level. Besides, closer striation lines next to the cracks were revealed a slower crack propagation rate compared to the unburnished sample tested at high fatigue stress.

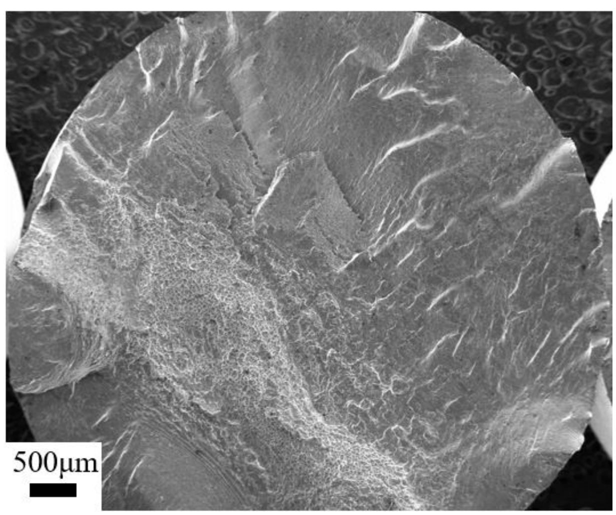

Figure 27: General view of the fatigue fracture surface of unburnished DSS sample broken in 36.832 cycles, at 95% of σ_{yield}.

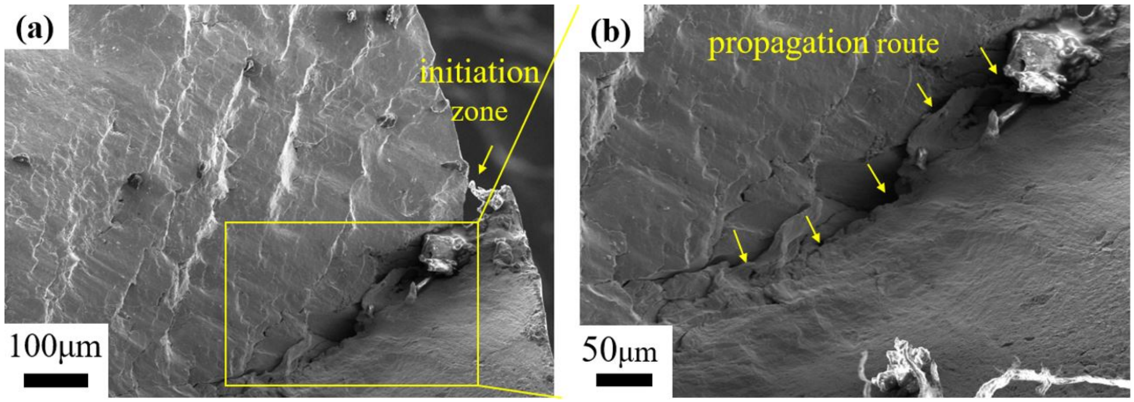

Figure 28: The fatigue fracture surface of unburnished DSS sample broken in 36.832 cycles, at 95% of σ_{yield} (a) crack initiation zone, (b) crack propagation.

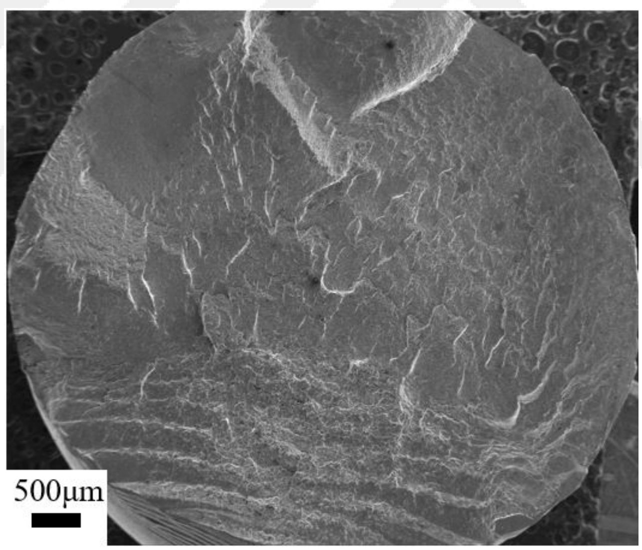

Figure 29: General view of the fatigue fracture surface of unburnished DSS sample broken in 5.282.618 cycles at 75% of σ_{yield}

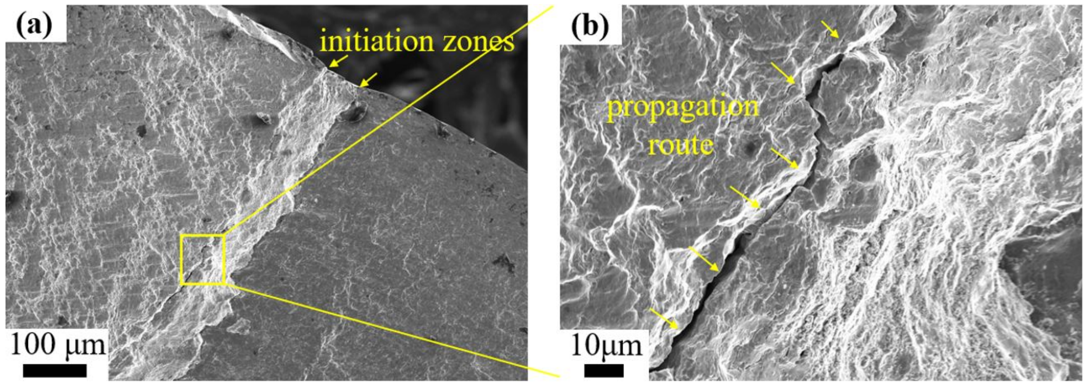

Figure 30: The fatigue fracture surface of unburnished DSS sample broken in 5.282.618 cycles at 75% of σ_{yield} (a) crack initiation zone, (b) crack propagation

Figures 31-34 demonstrate the fracture surface of condition R burnished samples tested at high and low stress amplitudes, respectively. Many fatigue crack progression zones detected on the fracture surface of the fatigued condition R sample tested in high stress amplitude due to high stress. As illustrated in Figure 32, despite the smooth surface and compressive residual stress, the cracks initiated from the surface of the sample that exposed high fatigue stress amplitude. This can be attributed to the high stress relaxation rate in the high fatigue stress amplitude of 840 MPa. A similar phenomenon was stated by Kim et al. [108] on the fatigue behavior of shot-peened medium-carbon steel.

Otherwise, due to the low surface roughness and compressive residual stress near the surface, the crack initiation zone shifted to the subsurface region in the sample tested at low stress amplitude (Figures 33-34). Furthermore, the cracks get thinner through the surface in relation to the high compressive residual stress near the surface. Besides, as indicated with small arrows, several internal cracks observed about 1 mm beneath the surface which may be linked to microstructure inhomogeneity and coarser grains under the refined surface layer [109, 110].

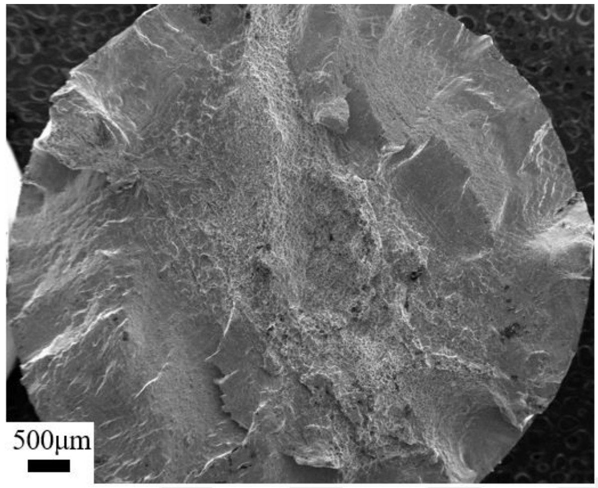

Figure 31: General view of the fatigue fracture surface of condition R DSS sample broken in 45.432 cycles, tested at 95% of σ_{yield}.

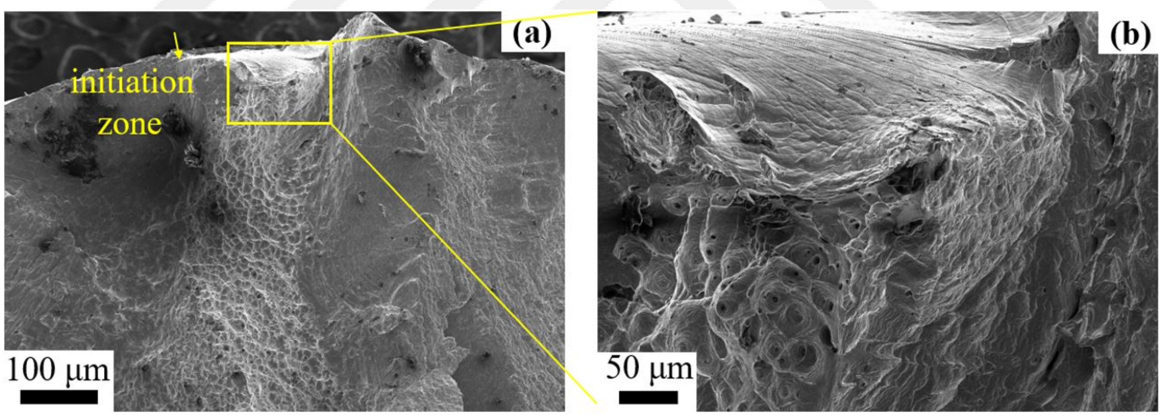

Figure 32: The fatigue fracture surface of condition R DSS sample broken in 45.432 cycles, tested at 95% of σ_{yield} (a) crack initiation zone, (b) crack propagation.

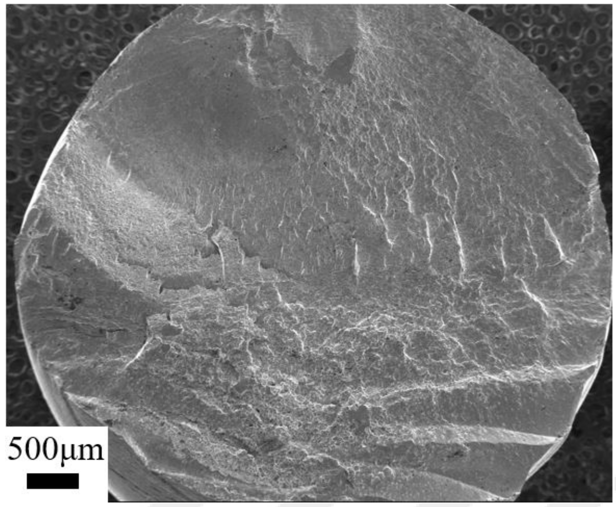

Figure 33: General view of the fatigue fracture surface of condition R DSS sample broken in 7.207.187 cycles, at 75% of σ_{yield}.

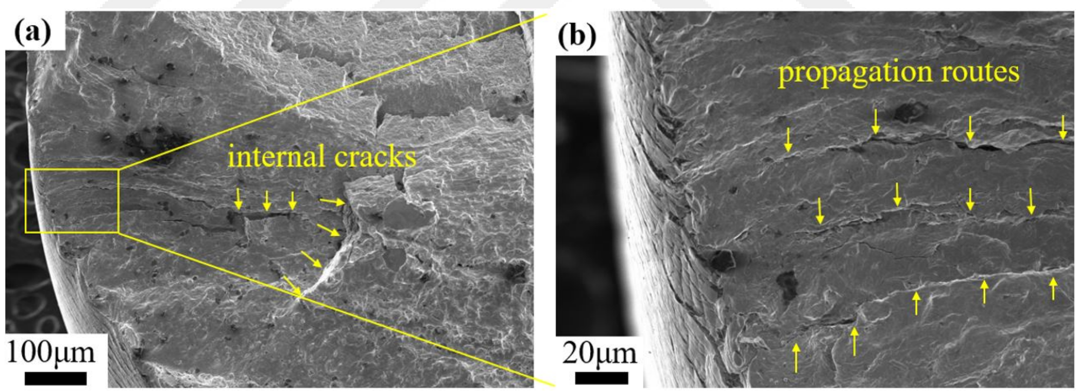

Figure 34: The fatigue fracture surface of condition R DSS sample broken in 7.207.187 cycles, at 75% of σ_{yield} (a) crack initiation zone, (b) crack propagation

Figures 35-38 represent the fracture surface of condition H burnished samples fatigued under the high and low stress amplitudes, respectively. As shown in Figure 37, the fatigue crack initiated from the surface due to relatively high surface roughness and relaxation of the compressive residual stress at the high stress amplitude level. Furthermore, internal crack originated from the microstructure inhomogeneity below the refined layer was detected similar to the fatigued condition R sample.

On the other hand, for the sample tested at low stress amplitude, the crack initiation zone shifted beneath the surface due to the high amount of compressive residual stress near the surface (Figure 38). Furthermore, multiple crack initiation zones detected below the surface and striation marks were observed started from the surface cracks and propagated to the inside of the sample indicating the fatigue fracture of the sample at low stress amplitude.

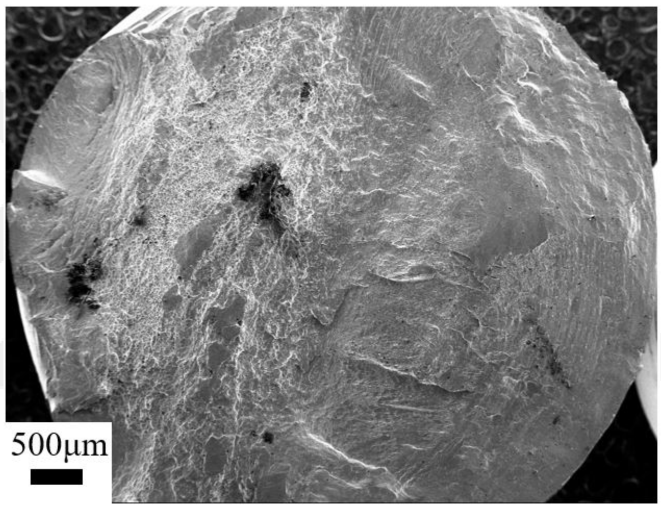

Figure 35: General view of the fatigue fracture surface of condition H DSS sample broken in 87.215 cycles, at 95% of σ_{yield}

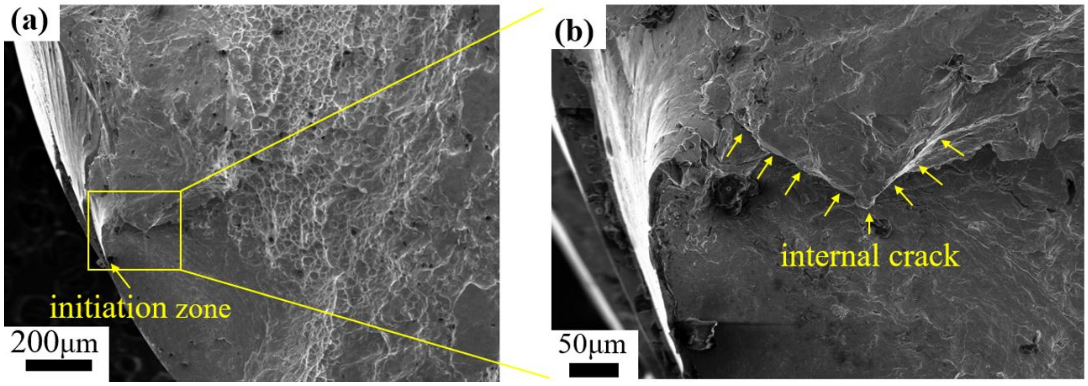

Figure 36: The fatigue fracture surface of condition H DSS sample broken in 87.215 cycles, at 95% of σ_{yield} (a) crack initiation zone, (b) internal crack.

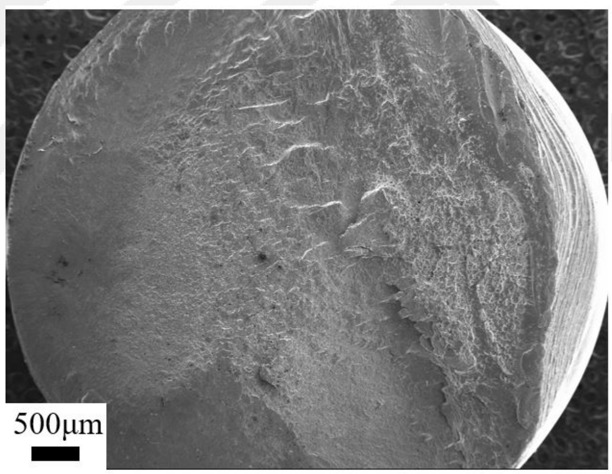

Figure 37: General view of the fatigue fracture surface of condition H DSS sample broken in 5.072.316 cycles, at 80% of σ_{yield}.

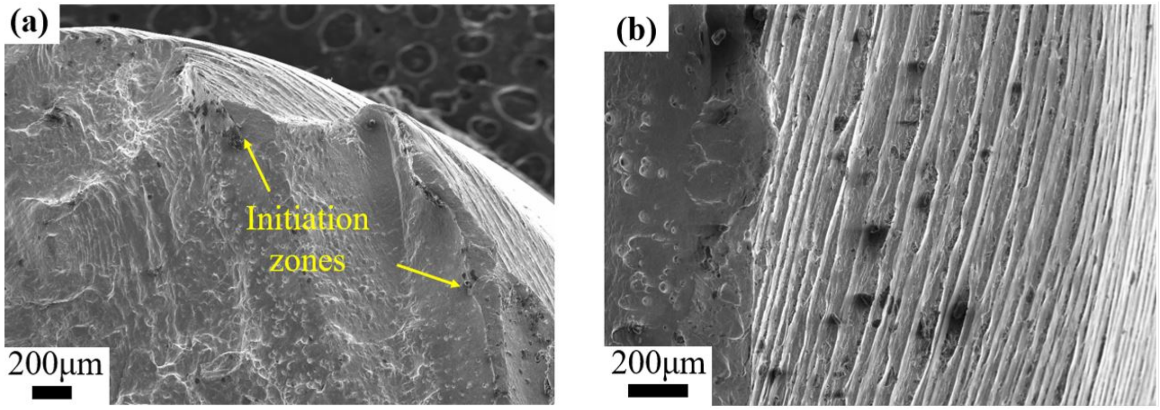

Figure 38: The fatigue fracture surface of condition H DSS sample broken in 5.072.316 cycles, at 80% of σ_{yield} (a) crack initiation zone, (b) striation lines.

The analyses of the fracture surfaces reveals that high compressive residual stress has a vital role in the enhancement in the fatigue life of DSS. However, in high stress amplitude, the enhancement in fatigue life is limited due to high stress relaxation. Besides, low surface roughness reduces stress concentration zones on the surface and improves fatigue life.

5.4 Results and Analysis on Wear Characteristics

Figure 39 shows the results of wear tests in the case of weight loss and wear resistance for DSS. The wear resistance of the condition H sample increased by up to 108% compared to the machined samples. The enhancement in the wear resistance can be explained by the low surface roughness and high hardness in the work-hardened layer. Also, wear resistance of condition H sample improved about 30% from the normal of 10N to 40N.

For soft abrasive cases, condition R sample has the highest wear resistance due to its low surface roughness. A smooth surface decreases localized stress in the mating area and lowers the loss of material on the surface. On the other hand, under hard abrasive conditions, condition H sample has the highest wear resistance. The high amount of compressive residual stress decelerates crack inhibition and propagation due to wear. Nevertheless, work hardening usually increases brittleness and lowers wear resistance but the increase must be too low due to superficial work hardening. Additionally, wear resistance rises with increasing distance and normal force for machined DSS samples because of work-hardening induced by the abrasive material. On the contrary, the situation is the opposite for the burnished samples. The work-hardened layer of burnished samples worn and disappears in long-distance tests.

Figure 40 represents the friction coefficient-distance graphs of DSS samples. In the first meters of the test, the condition R samples have the lowest coefficient due to the smooth surface. The surface with low asperities lowers friction and wear loss, subsequently increases wear resistance. That is why condition R samples have the highest wear resistance in the first half of the wear tests with a normal force of 10N (Figure 39a). However, as the test advances, the surface wears out and the friction coefficient becomes approximately equal for all conditions. Also, the coefficients tend to rise as the test advances. This situation can be attributed to the wearing of the abrasive material although no visual damage was detected.

The result of wear and fatigue test results revealed that the unburnished DSSs have the lowest wear resistance and fatigue life. That can be explained by high surface roughness and low compressive residual stress in the surface layer of unburnished DSS [111, 71]. Fatigue and fretting wear cracks initiate on the surface and propagate at a high rate for unburnished DSS. On the other hand, crack propagation rate is low for condition H DSS due to compressive residual stress induced.

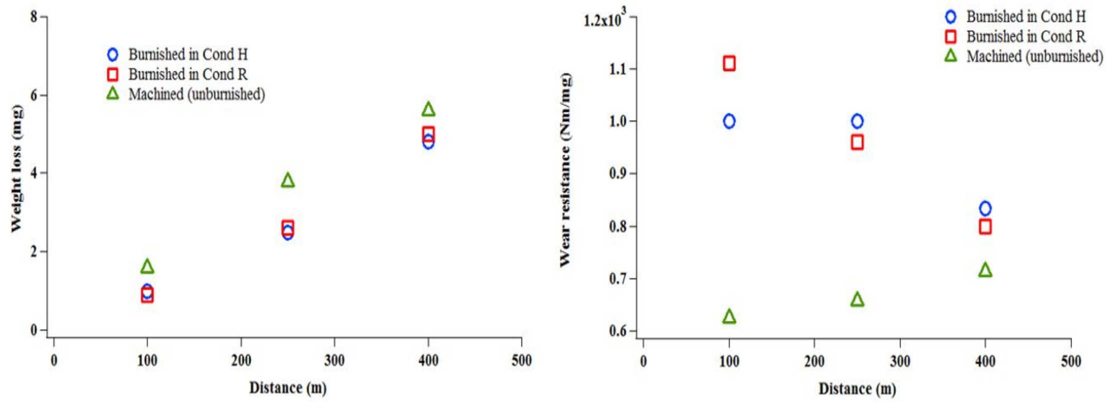

(a)

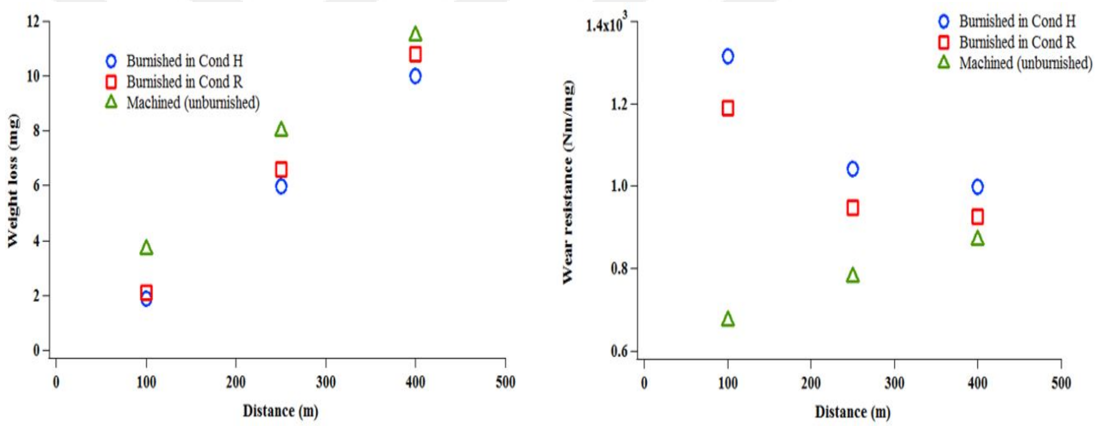

(b)

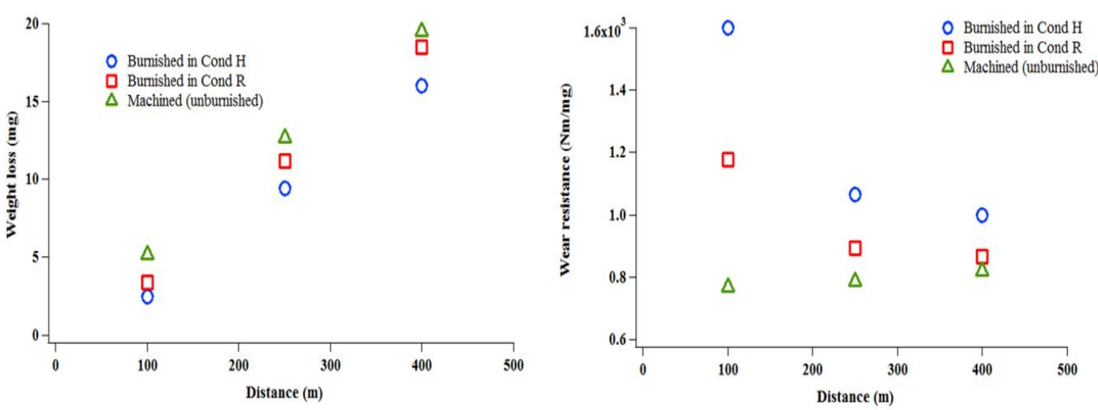

(c)

Figure 39: Weight loss and wear resistance relationship to the sliding distances for DSS at a) $F_N = 10$N, b) $F_N = 25$N, c) $F_N = 40$N.

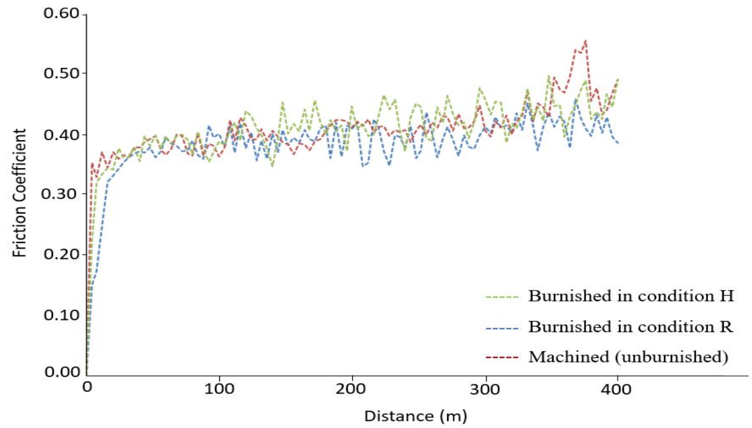

(a)

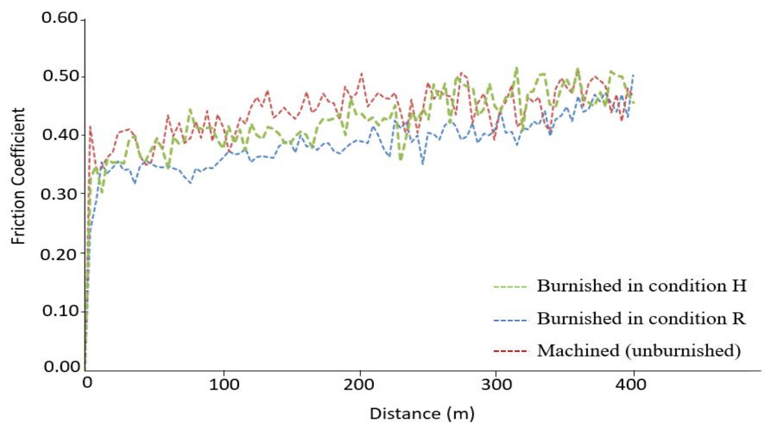

(b)

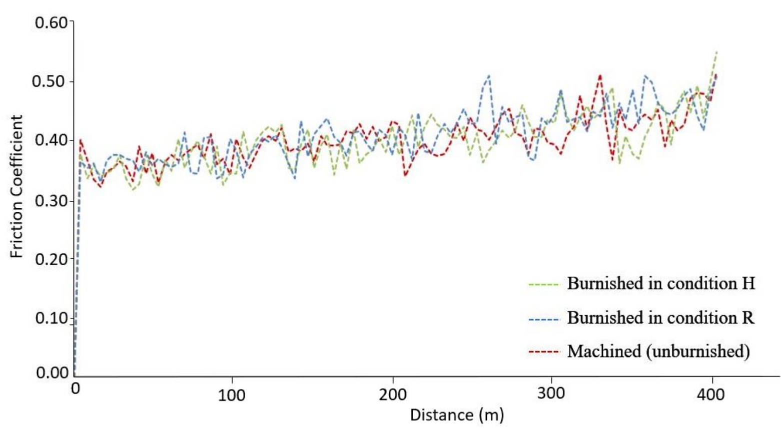

(c)

Figure 40: Friction coefficient changes for DSS at a) $F_N = 10$N, b) $F_N = 25$N, c) $F_N = 40$N.

5.4.1 Wear Track Analyses

Figure 41 shows the microscopic images of the wear tracks of the worn DSS samples after a test distance of 400m. An abrasive deformation mode and ploughing was observed, which led to grooves in the sliding direction. Abra-Arzola et al. [112] reported wear cracks perpendicular to the sliding direction of worn DSS by SEM. Also, Liang et al. [113] reported compressive residual stress in the surface layer could impede crack formation during wear. As expected, the width of the grooves enlarged with the rise in normal load.

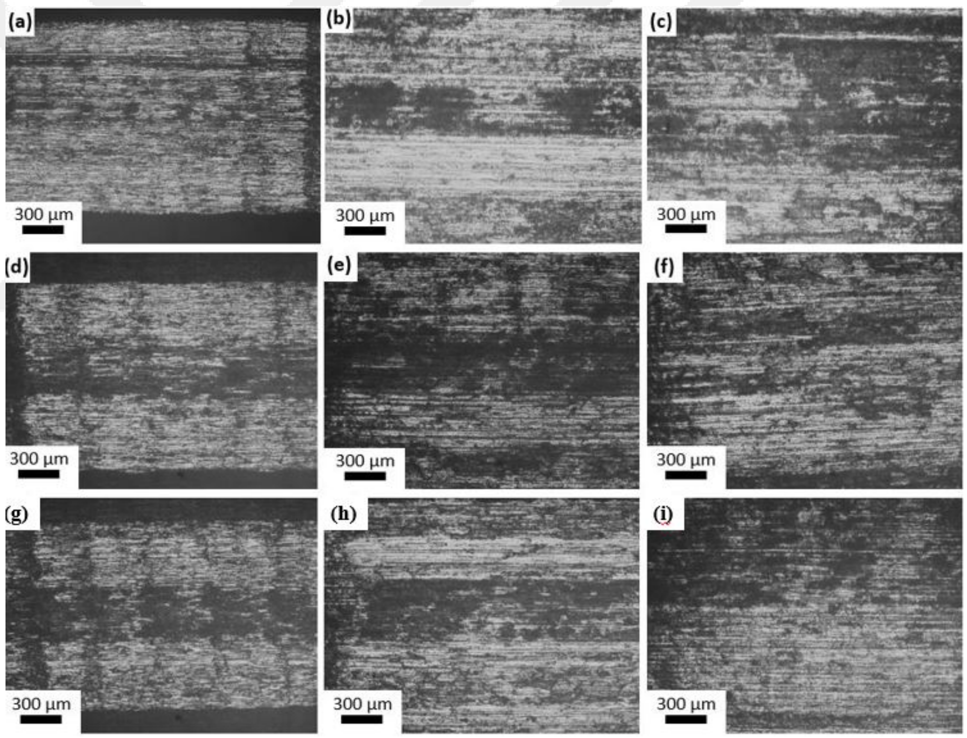

Figure 41: Optical micrographs showing the wear tracks of DSS after distance of 400N a) Unburnished Fw=10N, b) Unburnished Fw=25N, c) Unburnished Fw=40N, d)Condition R Fw=10N, e) Condition R Fw=25N, f) Condition R Fw=40N g) ConditionH Fw=10N h) Condition H Fw=25N, i) Condition H Fw=40N

CHAPTER VI

EFFECT OF BURNISHING ON THE FATUGUE LIFE AND WEAR BEHAVIOR OF 316L STAINLESS STEELS

6.1 Results and Analysis on Monotonic Mechanical Behaviour

Figure 42a and b represent stress-strain curves of unburnished and condition H 316L samples, respectively. Tensile strength rose about 1.5%, however, yield strength almost stayed at the same level. Tensile strengths are 765 Mpa and 777 MPa and yield strengths are 600 MPa and 602 MPa, respectively for unburnished and condition H 316L samples. The changes are negligible due to the superficiality of the burnishing process. Similarly, Aviles et al. [76] reported no change in tensile strength of AISI 1045 steel after the ball burnishing process. Furthermore, percent elongation at fracture was 58.12% and 62.24%, respectively for unburnished and condition H 316L samples.

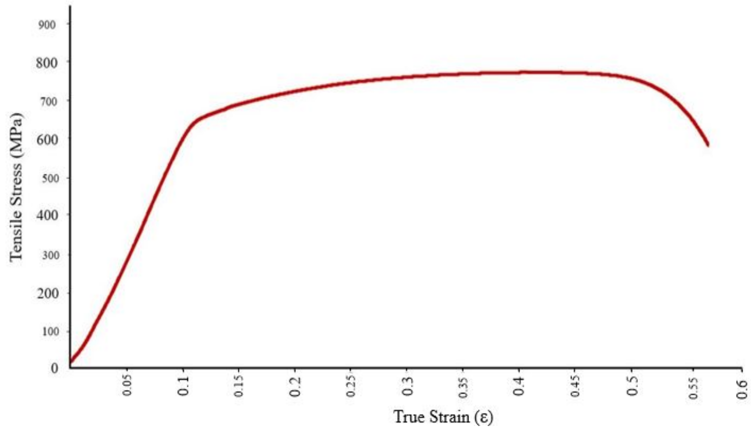

(a)

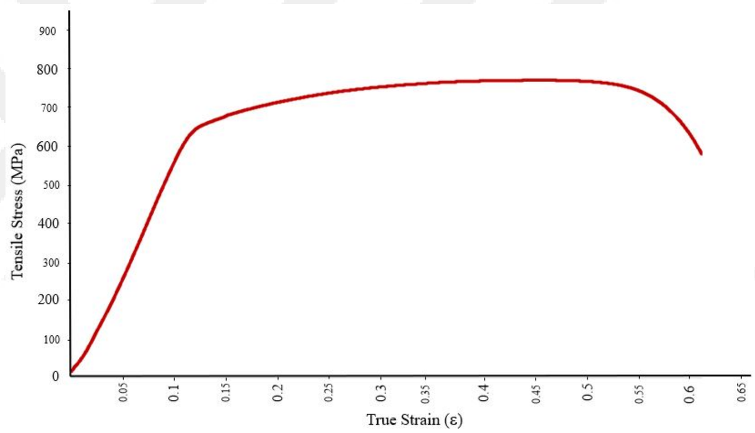

(b)

Figure 42: Stress-Strain curves of a) Unburnished 316L, b) Condition H 316L.

6.2 Results and Analysis on HCF Life

Figure 43 shows the results of the HCF tests of 316L samples on a semi-log scale and the arrows indicate run outs. It is clear that burnishing increased fatigue life of 316L significantly, especially at low fatigue stress amplitudes. The main factor for that rise is compressive residual stress that was induced by Inspection of data gathered from the S-N curve was revealed that at high-stress amplitude, the fatigue life of the Condition R sample is nearly equal to that of the unburnished sample despite low surface roughness. This can be explained with the high-stress relaxation rate at high stress amplitude [79] and the low amount of compressive residual stress induced by the burnishing. Similar results were reported by Denkena et al. [114] for the fatigue life of burnished magnesium alloy. On the other hand, condition H samples have significantly improved fatigue life due to high amount of compresive residual stress induced.

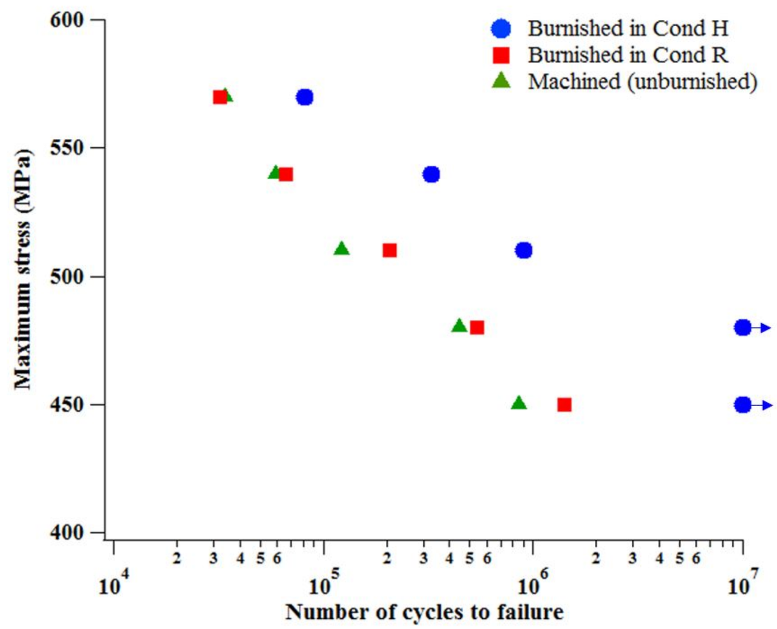

Figure 43: HCF results of the unburnished, condition R and condition H 316L samples (arrows indicate run outs)

Comparing the fatigue life of DSS and 316L samples, it was observed that the improvement in the fatigue life of condition R 316L samples is limited, especially at high fatigue stress amplitude. This situation can be attributed to the low depth of the work hardened surface layer of condition R 316L compared to that of DSS (Figure 17 and 18). For condition R 316L, fatigue cracks initiated in the subsurface region and propagated through the center at a high propagation rate due to low compressive residual stress in the subsurface layer beneath 0.2 mm. Similarly, it was disclosed that the low depth of compressive residual stress limits the increase in fatigue life after mechanical surface treatment [115, 116]. On the other hand, the burnished samples except condition R 316L have improved fatigue life, especially condition H burnished ones.

6.2.1 Fracture Morphology Analysis of 316L Stainless Steel

Figures 44-55 represent the fracture surfaces of the fatigue failed 316L samples those were tested at high and low-stress amplitudes, respectively. High tears density is illustrated in Figure 44, which represents fatigue fracture mode for the unburnished sample that was exposed to high-stress amplitude. The fatigue crack initiated on the surface and propagated through the center.

Similarly, the sample tested at low-stress amplitude was fractured due to fatigue rupture mode (Figure 46). However, closer striation lines in the fatigue fractured zone reveal a slower crack propagation rate compared to the unburnished sample tested at high-stress amplitude. Also, the final fracture section of the sample represents a more ductile rupture than the unburnished sample tested at high-stress amplitude.

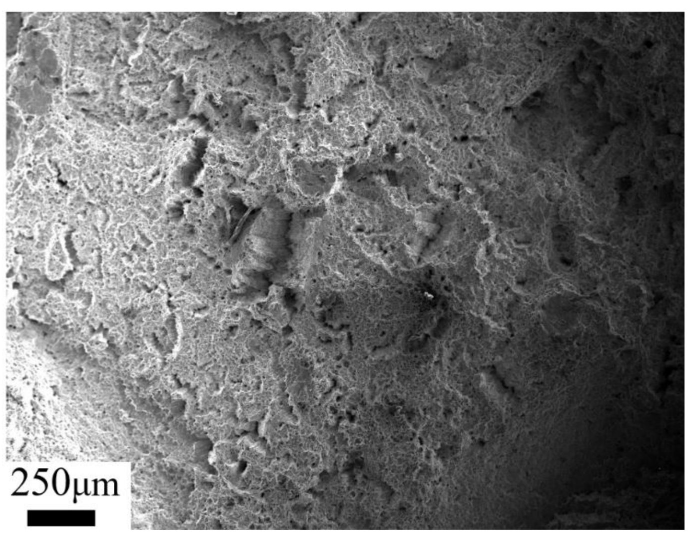

Figure 44: General view of the fatigue fracture surface of unburnished 316L sample broken in 33.842 cycles, at 95% of σ_{yield}.

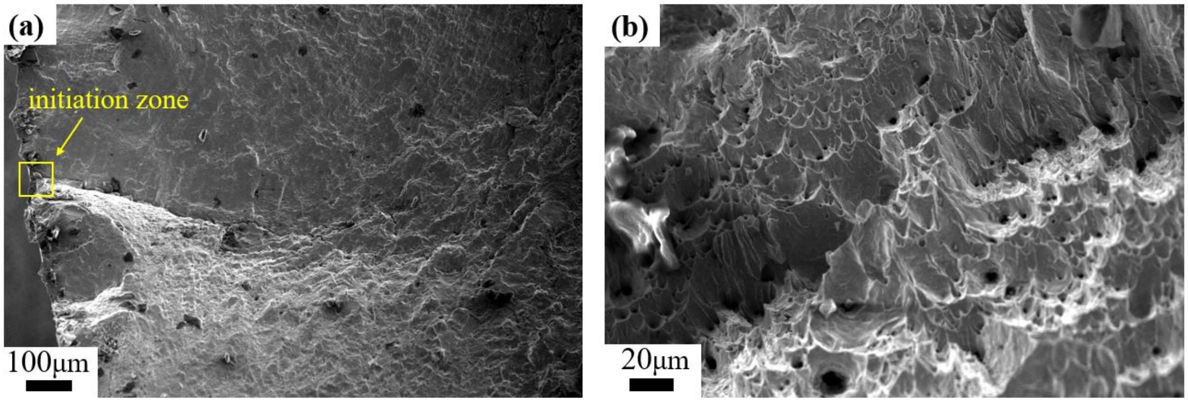

Figure 45: The fatigue fracture surface of unburnished 316L sample broken in 33.842cycles, at 95% of σ_{yield} (a) crack initiation zone, (b) Tearing zone.

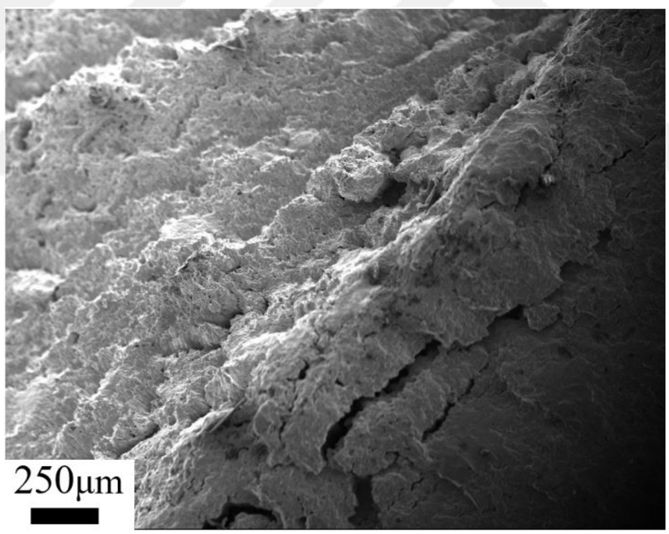

Figure 46: The fatigue fracture surface of unburnished 316L sample broken in 849.625 cycles, at 75% of σ_{yield}.

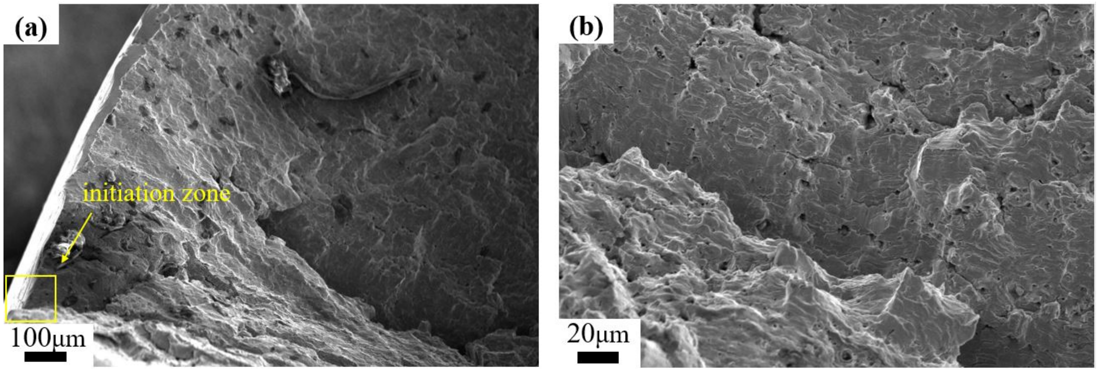

Figure 47: The fatigue fracture surface of unburnished 316L sample broken in 849.625 cycles, at 75% of σ_{yield} (a) crack initiation zone, (b) Crack propagation.

Figures 48-51 show the fracture surface of condition R 316L samples those were tested at high and low-stress amplitudes, respectively. As demonstrated in Figure 49 the fatigue crack has started on the surface, similar to the condition R DSS sample, due to the high stress relaxation rate. Furthermore, internal microcracks were observed about 0.9 mm beneath the surface. This situation can be connected to poor microstructure beneath the work-hardened layer.

Otherwise, the crack initiation zone shifted about 0.2 mm beneath the surface for the sample that was tested in low-stress amplitude (Figure 51). The crack propagated towards both the center and the surface of the material. Also, internal cracks were tracked. Moreover, equiaxed and deep dimples represent ductile final rupture.

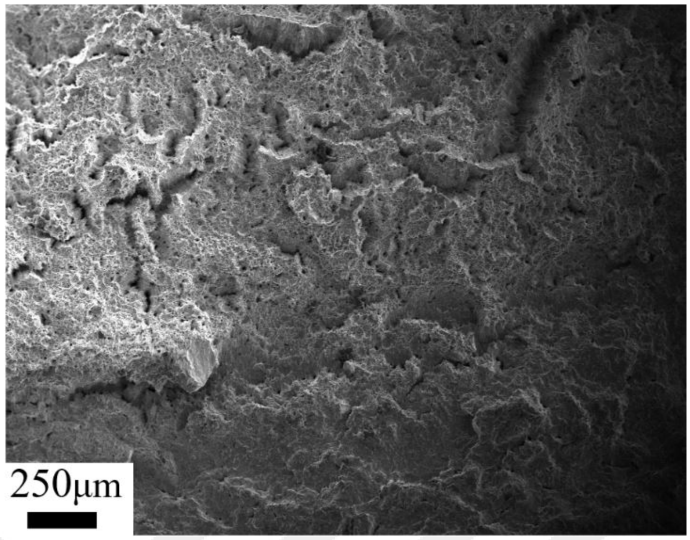

Figure 48: General view of the fatigue fracture surface of condition R 316L sample broken in 31.956 cycles, at 95% of σ_{yield}.

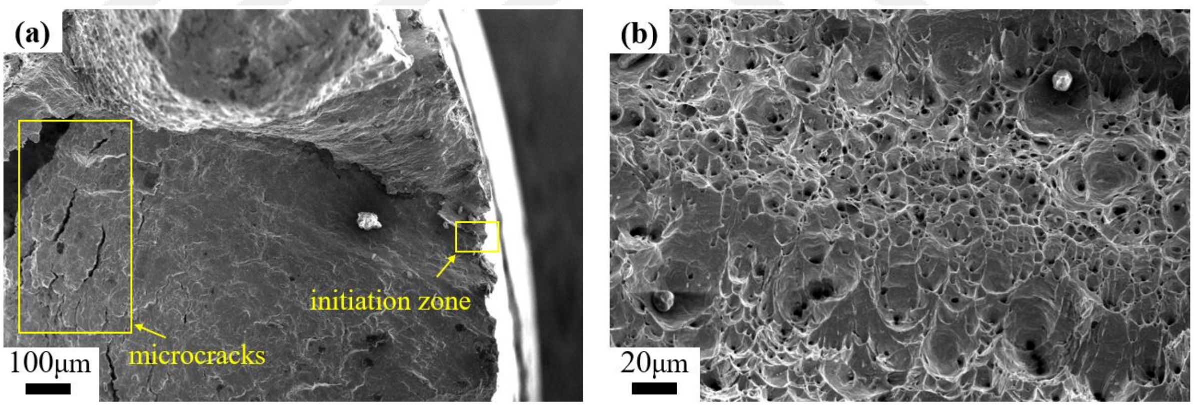

Figure 49: The fatigue fracture surface of condition R 316L sample broken in 31.956 cycles, at 95% of σ_{yield} (a) crack initiation zone, (b)Final rupture zone.

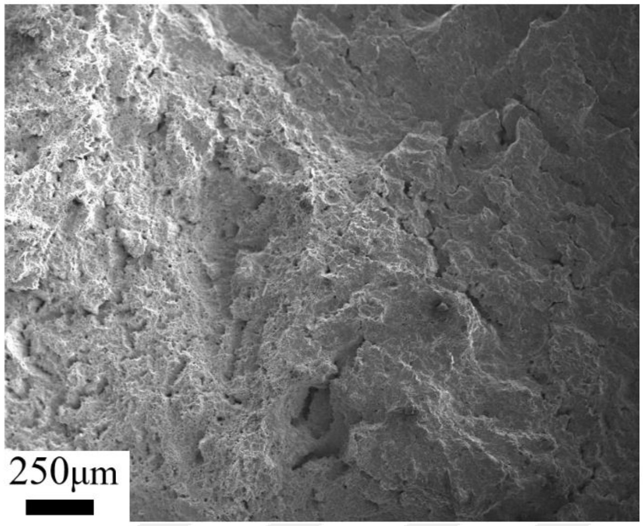

Figure 50: General view of the fatigue fracture surface of condition R 316L sample broken in 1.400.365 cycles, at 75% of σ_{yield}.

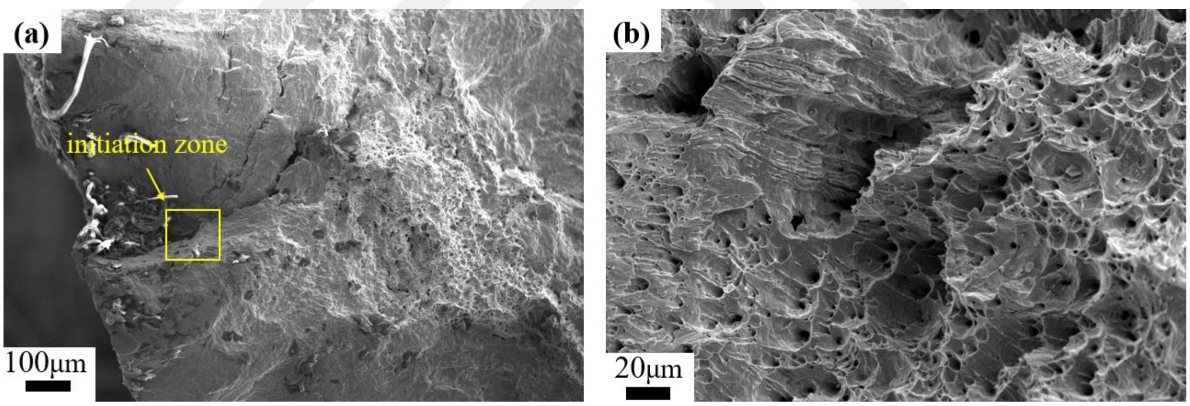

Figure 51: The fatigue fracture surface of condition R 316L sample broken in 1.400.365 cycles, at 75% of σ_{yield} MPa (a) crack initiation zone, (b)Final rupture zone.

Figures 52-55 demonstrate the fracture surface of condition H 316L samples those were tested at high and low-stress amplitudes, respectively. As demonstrated in Figure 53, the fatigue crack has started on the surface. This phenomenon can be explained by the deteriorated surface, high stress relaxation rate, and relatively high surface roughness. However, the crack propagation rate has decreased towards the center because of high compressive residual stress beneath the surface.

On the other hand, the crack initiated on the surface and propagated through the center for the sample that was exposed to low-stress amplitude (Figure 55). However, due to lower stress, the propagation rate to is lower compared to the sample that was exposed to high fatigue stress amplitude.

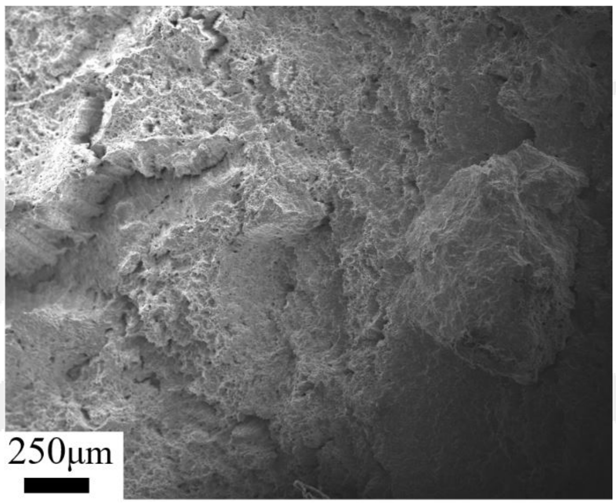

Figure 52: General view of the fatigue fracture surface of condition H 316L sample broken in 81.973 cycles, at 95% of σ_{yield}.

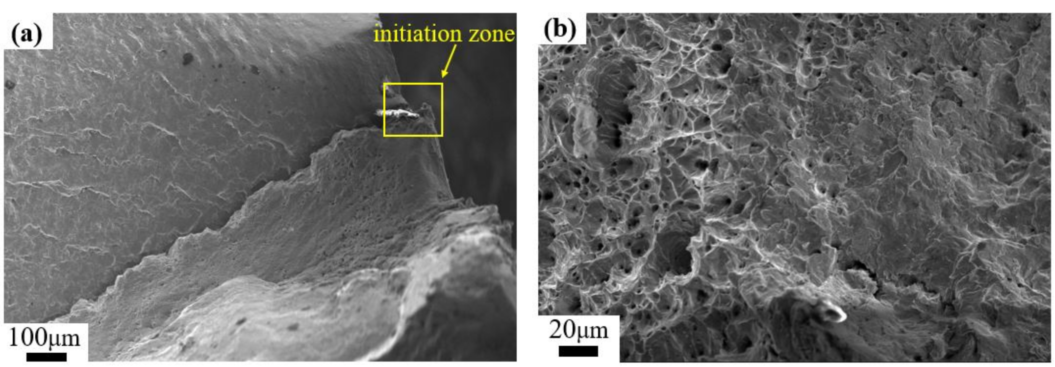

Figure 53: The fatigue fracture surface of condition H 316L sample broken in 81.973 cycles, at 95% of σ_{yield} (a) crack initiation zone, (b)Final rupture zone.

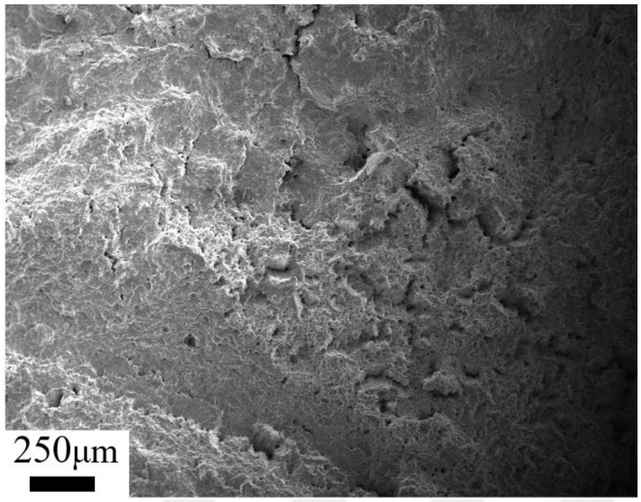

Figure 54: General view of the fatigue fracture surface of condition H 316L sample broken in 898.253 cycles, at 85% of σ_{yield}.

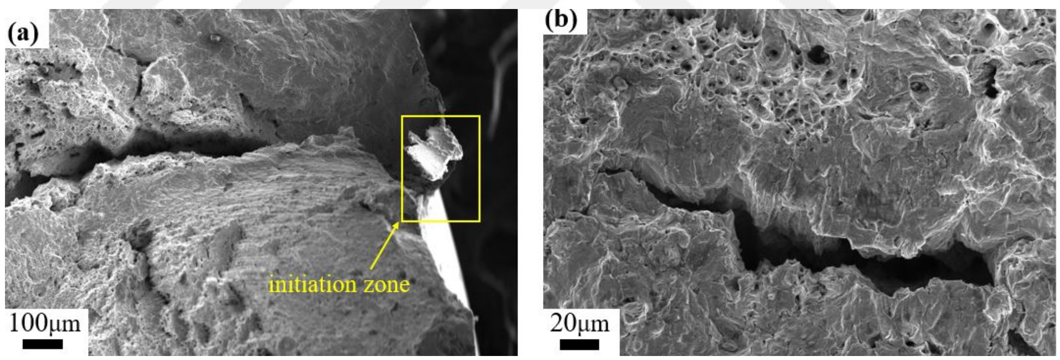

Figure 55: The fatigue fracture surface of condition H 316L sample broken in 898.253 cycles, at 85% of σ_{yield} (a) Crack initiation zone, (b) Crack propagation.

Low surface roughness and compressive residual stress induced by burnishing restricted crack initiation and propagation stages. On the other hand, cracks initiated on the surface for condition H burnished 316L samples due to surface deterioration. However, they could not propagate through the center rapidly due to high compressive residual stress beneath the surface.

Comparing the fracture surfaces of DSS and 316L samples, the crack initiation zone was shifted beneath the surface and the propagation rate decreased for burnished samples tested in low stress amplitude for both materials due to induced compressive residual stress. However, cracks started on the surface for condition H 316L because of surface deterioration. Also, internal cracks were observed beneath the surface for both materials, which could be connected to microstructural inhomogeneity and coarser grains under the refined surface layer [109, 110] Furthermore, high density line striations were observed on the fracture surface of DSS. This can be explained by the high plastic deformation attributed to the high ductility of DSS [117, 118]. Table 11 compares the fracture surface features of the fatigued samples.

Table 11: Features of the Fracture Surfaces

Condition		Unburnished	R	H
DSS	Low	Crack initiation on surface Moderate propagation rate Moderate plastic deformation	Crack initiation below surface Low propagation rate High plastic deformation	Crack initiation below surface Very low propagation rate High density striations High plastic deformation
	High	Crack initiation on surface Very high propagation rate	Crack initiation on surface High propagation rate High residual stress relaxation	Crack initiation on surface High propagation rate High residual stress relaxation
316L	Low	Crack initiation on surface Moderate propagation rate	Crack initiation below surface Low propagation rate	Crack initiation on surface Very low propagation rate
	High	Crack initiation on surface Very high propagation rate	Crack initiation on surface Very high propagation rate High residual stress relaxation	Crack initiation on surface High propagation rate High residual stress relaxation

6.3 Results and Analysis on Wear Characteristics

Figure 56 represents the results of the wear test for 316L samples. The wear resistance of 316L was enhanced significantly after the burnishing process. Wear resistance of condition H burnished 316L samples increased by up to 57% compared to the machined samples. Smooth surface and increased hardness are the main factors for that rise [88].

Wear resistance of condition R 316L samples in soft abrasive conditions is slightly higher than that of condition H 316L samples. This can be explained with the chattering phenomenon on the surface [119] and low microhardness in the subsurface layer of condition H sample (up to 0.1 mm). On the other hand, after the disappearance of this layer, the wear resistance of the condition H 316L sample increased significantly, which well agrees with the microhardness distribution of 316L (Figure 18). Wear resistance of all the samples has become almost equal after disappearance of the burnsihed affected layer, which strongly matches with the results of Sun et al. [120]. Furthermore, it was observed that wear resistance of burnished 316L was first increased, then decreased with distance for the normal force of 10N. On the other hand, the wear resistance of condition H 316L increased linearly for the normal force of 25N. This phenomenon can be explained by the deteriorated surface of condition H 316L and the low depth of compressive residual stress for condition R 316L compared to that of DSS. The layer just below the surface of condition H 316L worn rapidly due to its deteriorated surface, as that layer disappears the wear resistance increased significantly. Also, a higher rate of work-hardening was induced to 316L by the abrasive material compared to DSS due to a lower hardness of 316L. As the burnished surface layer was worn, the abrasive material created a new work hardened surface layer in low normal force. However, for the normal force of 40N wear resistance of the burnished samples diminished steadily due to the high amount of abrasion.

Figure 57 shows the friction coefficient - distance graphs of 316L samples. The coefficients of the burnished samples are lower than the unburnished ones due to low surface roughness. Also, low friction enhances the wear resistance of the condition R sample. As illustrated in Figure 56a and b, wear resistance of condition R samples are higher than that of condition H samples in the first half of the tests. This situation can be attributed to low friction and the deteriorated surface of condition H. Also, friction coefficients increase as the test advances.

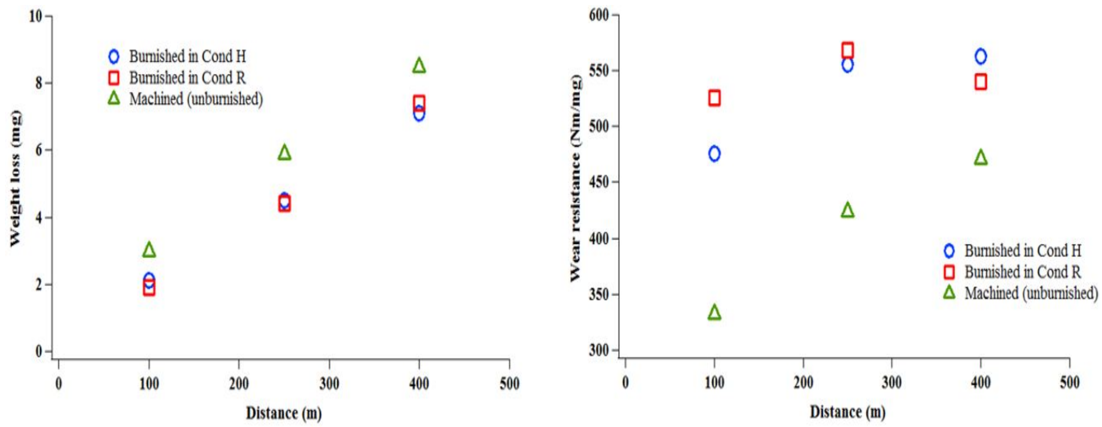

(a)

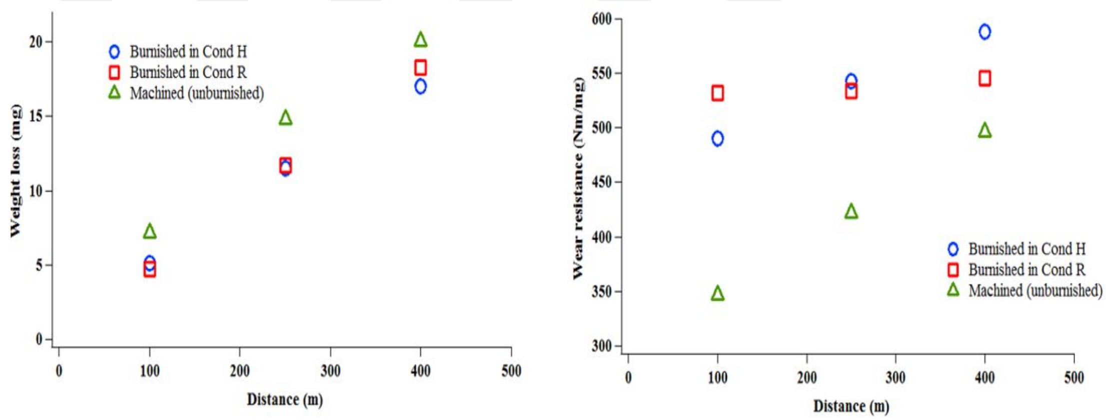

(b)

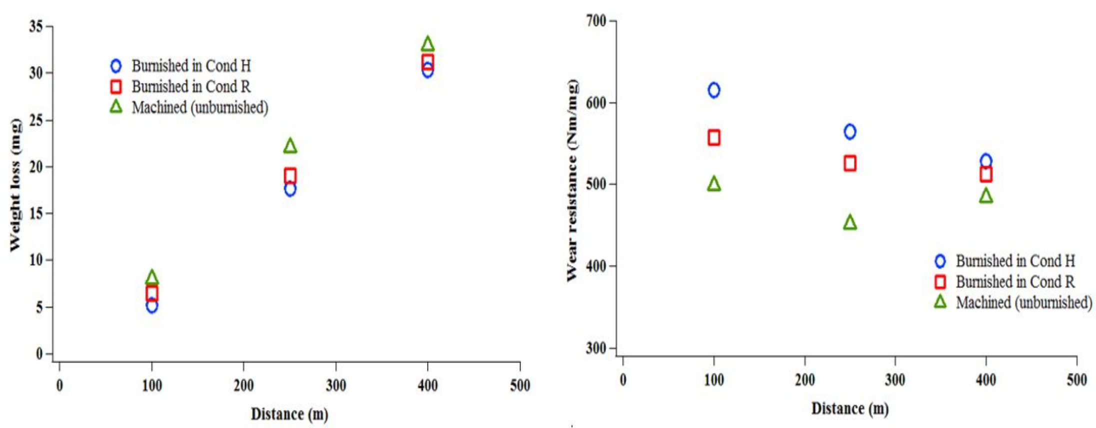

(c)

Figure 56: Weight loss and wear resistance relationship to the sliding distances for 316L at a) $F_N = 10$N, b) $F_N = 25$N, c) $F_N = 40$N.

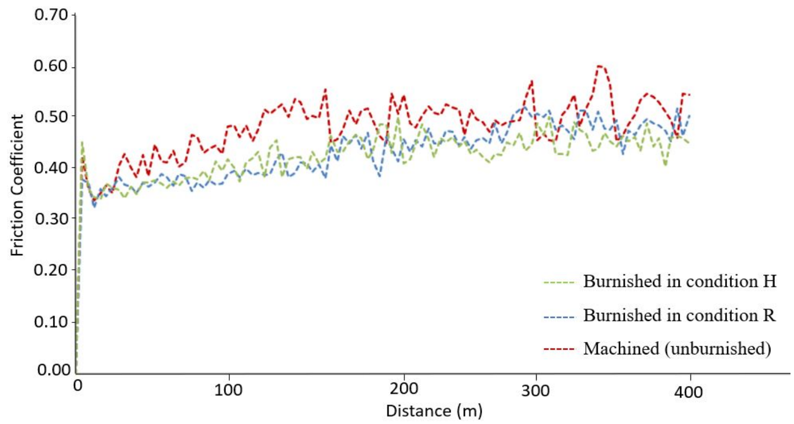

(a)

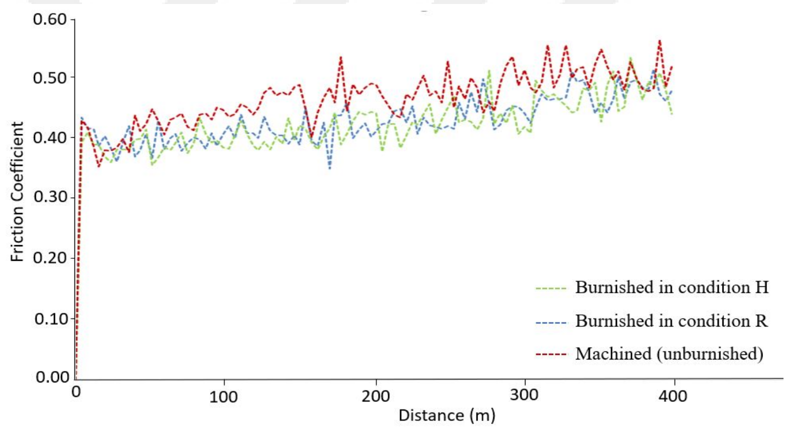

(b)

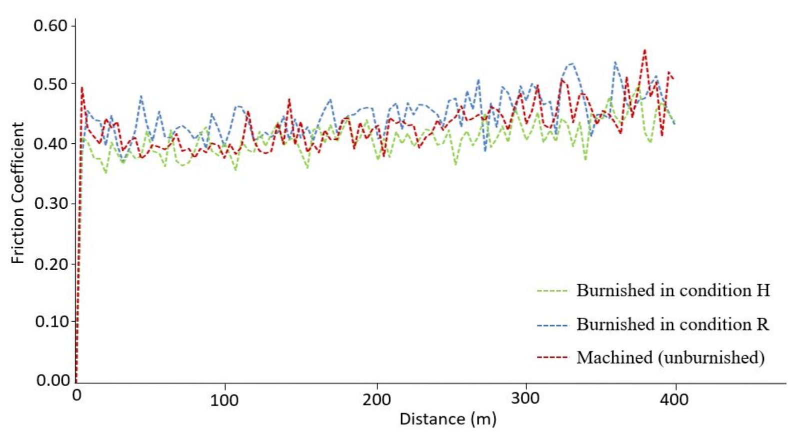

(c)

Figure 57: Friction coefficient changes for 316L at a)F_N= 10N, b)F_N= 25N, c)F_N= 40N.

Although the deteriorated surface of condition H 316L, it has superior wear and fatigue properties, while those of unburnished one is the lowest. Similarly, fracture surface analyses of fatigued condition H 316L revealed a low fatigue crack propagation rate. The high amount of compressive residual stress is the most influential factor since it lowers both fretting wear and fatigue crack propagation rate.

6.3.1 Analyses of Wear Track

Figure 58 represents the microscopic images of the wear tracks of worn 316L samples after a test distance of 400m, under different normal forces. As expected, the unburnished samples have the widest worn surface, and with the increase in normal load, the width of the damaged region enlarged, and the damage became more severe.

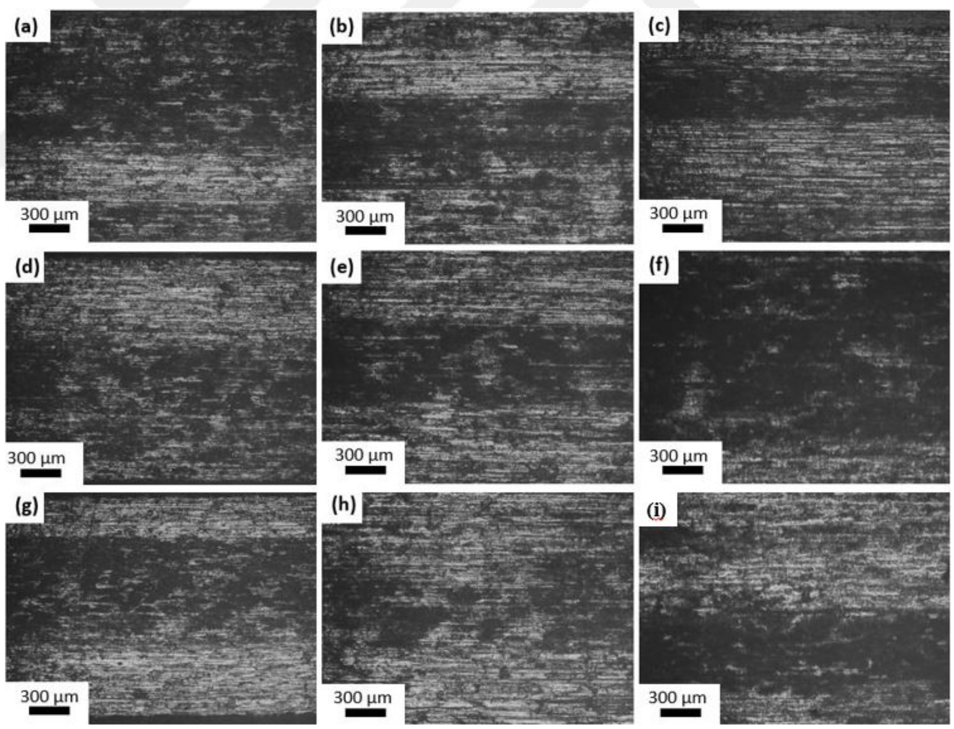

Figure 58: Optical micrographs showing the wear tracks of 316L after distance of 400N a) Unburnished Fw=10N, b) Unburnished Fw=25N, c) Unburnished Fw=40N, d) Condition R Fw=10N, e) Condition R Fw=25N f) Condition R Fw=40N, g) Condition H Fw=10N, h) Condition H Fw=25N, i) Condition H Fw=40N.

An abrasive wearing mechanism was observed on the wear surfaces, which is represented by the appearance of deep scars that resulted from scratching. Also, Peruzzo et al. [121] reported an oxidized layer on the worn surface of 316L by EDS mapping due to frictional heating in ambient air. Sun et al. described the dark regions as the rough surface. In some regions, the oxide film is removed to create wear debris, leaving after a dark and rough surface [122].

CHAPTER VII

CONCLUSION

This thesis is motivated to determine the effects of roller burnishing on Duplex Stainless Steel (DSS) and 316L stainless steel. Three different levels of force, feed, speed, and the number of passes have been utilized to find out the optimized burnishing parameters for the best surface integrity. Moreover, the fatigue life and wear resistance of burnished and machined samples were compared.

Significant enhancement in surface integrity was determined after the burnishing process. Notable reduction in surface roughness was achieved with the appropriate burnishing parameters. The results of microhardness tests revealed an remarkable increase in the microhardness of the surface and the surface layer. Furthermore, a notable grain refinement in the surface layer was observed with a decreasing rate from the surface through the center of the burnished samples.

After burnishing, the tensile and yield strengths did not change due to the superficial process. However, notable improvements were determined in fatigue life and wear resistance of the burnished samples.

For DSS, the lowest surface roughness was reached with low burnishing force, low feed rate, low spindle speed and a high number of passes (Force=500N, feed=0,1mm/rev, pass=3, speed=300rpm), and this parameter combination was named as condition R. The surface roughness of condition R DSS has decreased by 60%. Furthermore, the maximum microhardness was obtained with high burnishing force, low feed, low spindle speed and a high number of passes (Force=1500N, feed=0,1mm/rev, pass=3, speed=300rpm), and the parameter combination was named as condition H. Microhardness of the condition H DSS increased by 18%. Also, speed can be described as an ineffective parameter on both roughness and hardness, since its effect is too low and inconsistent.

The cyclic performance of the burnished samples for both optimized conditions was better than that of the machined condition. Also, the fatigue life of condition H burnished sample was significantly higher than other samples at all stress amplitude levels due to the induced compressive residual stress. However, the level of enhancement was lower for the samples fatigued at high fatigue stress amplitudes attributed to high stress relaxation rate. The fracture surface observation was revealed that the crack initiation zones were shifted below the surface due to the low surface roughness and compressive residual stress, which restricts the crack initiation and propagation stages. Moreover, the wear resistance of the burnished samples for both optimized conditions was higher than that of the machined condition. In soft abrasive conditions, the condition R DSS has the highest wear resistance due to its low surface roughness. In contrast, in hard abrasive conditions, condition H DSS samples were more resistive against wearing due to the high work hardening rate. The material loss decreased up to 32% compared to unburnished DSS. However, with increasing distance and contact stress, the hardened layer disappears, and wear resistance lowers.

For 316L, the lowest surface roughness was achieved after burnishing with the optimized parameter of condition R. Surface roughness reduced by 47% after burnishing with R parameter. Also, the highest surface microhardness was detected after burnishing with H parameter and microhardness increased by 45%. Nevertheless, low microhardness was detected just below the surface for condition H 316L.

The cyclic performance of 316L enhanced considerably after burnishing with the optimized parameters. It was observed that condition H 316L is the most durable sample against cyclic loading. The high level of compressive residual stress decelerated crack initiation and propagation. Furthermore, the fatigue life of condition R 316L samples have enhanced compared to the unburnished samples due to the low surface roughness and compressive residual stress induced. Furthermore, wear resistance of 316L improved after burnishing with the optimized parameters. Due to the surface deterioration of condition H 316L wear resistance of that sample is low in soft abrasive cases. Condition R 316L samples has the highest wear resistance in soft abrasive cases, however, in hard abrasive cases, condition H 316L samples are more resistive to wear. Similar to DSS cases, after the disappearance of the work hardenend layer, wear resistance of burnished 316L lowers.

The current experimental study revealed that roller burnishing enhances fatigue life and wear resistance of DSS and 316L. However, the parameters should be determined according to the hardnes of the workpiece. Burnishing increased the fatigue life of materials significantly for all optimized conditions. The rate of enhancement in the fatigue life of condition H 316L is higher than that of DSS. The endurance limit of 316L rose to about 85% of σ_{yield} for 316L; however, it raised to around 80% of σ_{yield} for DSS after burnishing with the condition H parameter. That can be attributed to the higher work hardening induced to 316L, despite the deteriorated surface. In addition, burnishing improved the wear resistance of the samples in most wearing cases. Also, the rate of enhancement in the wear resistance of the samples is close. However, the section with a low microhardness of condition H 316L wears faster and lowers the wear resistance of the sample in soft abrasive cases.

The current study revealed that roller burnishing process enhances cyclic and tribological properties by improving surface integrity in stainless steels. The process homogenizes microstructure in the surface layer and lowers surface roughness. Also, increased hardness and induced compressive residual stress, which arises after the process, is vital for high fatigue life and wear resistance. Especially, the high level of compressive residual stress increases fatigue life and wear resistance by restricting fatigue-fretting wear crack initiation and propagation.

Bibliography

[1] A. Griffith, "Philosophical transactions of the royal society of london," *Series A, containing papers of a mathematical or physical character*, vol. 221, pp. 163–198, 1921.

[2] H. Hertz, "Ueber die berührung fester elastischer körper.," *Journal für die reine und angewandte Mathematik*, vol. 1882, no. 92, pp. 156–171, 1882.

[3] A. C. Fischer-Cripps, *Introduction to contact mechanics*, vol. 101. Springer, 2007.

[4] K. Skalski, A. Morawski, and W. Przybylski, "Analysis of contact elastic-plastic strains during the process of burnishing," *International journal of mechanical sciences*, vol. 37, no. 5, pp. 461–472, 1995.

[5] J. E. Shigley, *Shigley's mechanical engineering design.* Tata McGraw-Hill Education, 2011.

[6] K. Johnson, "Contact mechanics cambridge univ," *Press, Cambridge*, vol. 95, p. 365, 1985.

[7] I. Altenberger, "Deep rolling–the past, the present and the future," in *Conf Proc: ICSP*, vol. 9, pp. 144–155, 2005.

[8] I. A. Scribner, "Burnishing-tool.," Feb. 8 1916. US Patent 1,171,146.

[9] P. Prabhu, S. Kulkarni, and S. Sharma, "Influence of deep cold rolling and low plasticity burnishing on surface hardness and surface roughness of aisi 4140 steel," *World Academy of Science, Engineering and Technology*, vol. 72, pp. 619–624, 2010.

[10] L. Luca, "Investigations into the use of ball-burnishing of hardened steel components as a finishing process.," 2003.

[11] P. S. Prevéy, N. Jayaraman, and J. Cammett, "Overview of low plasticity burnishing for mitigation of fatigue damage mechanisms," tech. rep., LAMBDA RESEARCH CINCINNATI OH, 2005.

[12] J. E. Scheel and D. J. Hornbach, "The effect of surface enhancement on improving the fatigue and sour service performance of downhole tubular components," in *ASME 2012 International Mechanical Engineering Congress and Exposition*, pp. 497–504, American Society of Mechanical Engineers Digital Collection, 2012.

[13] S. Neagu-Ventzel, *A theoretical and experimental study of single roll burnishing process as applied to yokes.* PhD thesis, University of Toledo, 2001.

[14] G. E. Dieter and D. Bacon, *Mechanical metallurgy*, vol. 3. McGraw-hill New York, 1986.

[15] P. S. Prevéy, "The measurement of subsurface residual stress and cold work distributions in nickel base alloys," in *ASMs conference on residual stress in design, process and materials selection*, pp. 11–20, 1987.

[16] T. Zhang, *The effects of ball burnishing for aerospace blade material 17-4 PH steel*. PhD thesis, University of Toledo, 2013.

[17] J. Maximov, G. Duncheva, A. Anchev, and M. Ichkova, "Slide burnishingre-view and prospects," *The International Journal of Advanced Manufacturing Technology*, vol. 104, no. 1-4, pp. 785–801, 2019.

[18] K. H. Lo, C. H. Shek, and J. Lai, "Recent developments in stainless steels," *Materials Science and Engineering: R: Reports*, vol. 65, no. 4-6, pp. 39–104, 2009.

[19] J. Olsson and M. Liljas, "years of dss applications," in *NACE Corrosion 94 Conf, paper*, no. 395, 60.

[20] K. Yurtışık, "Kinetics and microstructural analysis of fatigue fracture progress in weld joints of duplex stainless steel grade 2205," 2013.

[21] M. Field and J. Kahles, "The surface integrity of machined-and ground high-strength steels(surface integrity of machined and ground high strength steels)," *1964.*, pp. 54–77, 1964.

[22] D. Mahajan and R. Tajane, "A review on ball burnishing process," *International Journal of Scientific and Research Publications*, vol. 3, no. 4, pp. 1–8, 2013.

[23] M. El-Khabeery and M. El-Axir, "Experimental techniques for studying the effects of milling roller-burnishing parameters on surface integrity," *International Journal of machine tools and manufacture*, vol. 41, no. 12, pp. 1705–1719, 2001.

[24] E. K. Henriksen, "Residual stresses in machined surfaces," ASME, 1948.

[25] M. El-Axir, "A method of modeling residual stress distribution in turning for different materials," *International Journal of Machine Tools and Manufacture*, vol. 42, no. 9, pp. 1055–1063, 2002.

[26] G. E. Totten, *Handbook of residual stress and deformation of steel*. ASM international, 2002.

[27] P. R. Roberge, *Corrosion inspection and monitoring*, vol. 2. John Wiley & Sons, 2007.

[28] V. Raja and T. Shoji, *Stress corrosion cracking: theory and practice*. Elsevier, 2011.

[29] A. B. Rhouma, H. Sidhom, C. Braham, J. Lédion, and M. Fitzpatrick, "Effects of surface preparation on pitting resistance, residual stress, and stress corrosion cracking in austenitic stainless steels," *Journal of materials engineering and performance*, vol. 10, no. 5, pp. 507–514, 2001.

[30] A. Turnbull, K. Mingard, J. Lord, B. Roebuck, D. Tice, K. Mottershead, N. Fairweather, and A. Bradbury, "Sensitivity of stress corrosion cracking of stainless steel to surface machining and grinding procedure," *Corrosion science*, vol. 53, no. 10, pp. 3398–3415, 2011.

[31] E. Maawad, H.-G. Brokmeier, L. Wagner, Y. Sano, and C. Genzel, "Investigation on the surface and near-surface characteristics of ti–2.5 cu after various mechanical surface treatments," *Surface and Coatings Technology*, vol. 205, no. 12, pp. 3644–3650, 2011.

[32] N. Loh, S. Tam, and S. Miyazawa, "Investigations on the surface roughness produced by ball burnishing," *International Journal of Machine Tools and Manufacture*, vol. 31, no. 1, pp. 75–81, 1991.

[33] M. Salahshoor and Y. Guo, "Surface integrity of magnesium-calcium implants processed by synergistic dry cutting-finish burnishing," *Procedia Engineering*, vol. 19, pp. 288–293, 2011.

[34] A. Akkurt, "Comparison of roller burnishing method with other hole surface finishing processes applied on aisi 304 austenitic stainless steel," *Journal of materials engineering and performance*, vol. 20, no. 6, pp. 960–968, 2011.

[35] M. Mhaede, Y. Sano, I. Altenberger, and L. Wagner, "Fatigue performance of al7075-t73 and ti-6al-4v: comparing results after shot peening, laser shock peening and ball-burnishing," *Int J Struct Int*, vol. 2, no. 2, pp. 185–199, 2011.

[36] D. Shivalingappa *et al.*, "The influence of ball and roller burnishing process parameters on surface integrity of al 2024 alloy," *Materials Today: Proceedings*, 2020.

[37] F. Klocke and J. Liermann, "Roller burnishing of hard turned surfaces," *International Journal of Machine Tools and Manufacture*, vol. 38, no. 5-6, pp. 419–423, 1998.

[38] L. L. De Lacalle, A. Lamikiz, J. Sánchez, and J. Arana, "The effect of ball burnishing on heat-treated steel and inconel 718 milled surfaces," *The International Journal of Advanced Manufacturing Technology*, vol. 32, no. 9-10, pp. 958–968, 2007.

[39] A. Rodríguez, L. L. de Lacalle, A. Celaya, A. Lamikiz, and J. Albizuri, "Surface improvement of shafts by the deep ball-burnishing technique," *Surface and Coatings Technology*, vol. 206, no. 11-12, pp. 2817–2824, 2012.

[40] A. Saldaña-Robles, H. Plascencia-Mora, E. Aguilera-Gómez, A. Saldaña-Robles, A. Marquez-Herrera, and J. A. Diosdado-De la Peña, "Influence of ball-burnishing on roughness, hardness and corrosion resistance of aisi 1045 steel," *Surface and Coatings Technology*, vol. 339, pp. 191–198, 2018.

[41] L. L. De Lacalle, A. Lamikiz, J. Muñoa, and J. Sánchez, "Quality improvement of ball-end milled sculptured surfaces by ball burnishing," *International Journal of Machine Tools and Manufacture*, vol. 45, no. 15, pp. 1659–1668, 2005.

[42] F. L. Li, W. Xia, Z. Y. Zhou, J. Zhao, and Z. Q. Tang, "Analytical prediction and experimental verification of surface roughness during the burnishing process," *International Journal of Machine Tools and Manufacture*, vol. 62, pp. 67–75, 2012.

[43] M. Prevey and P. S. Prevey III, "Burnishing tool and method for burnishing," Dec. 10 2013. US Patent 8,601,659.

[44] T. El-Taweel and M. El-Axir, "Analysis and optimization of the ball burnishing process through the taguchi technique," *The International Journal of Advanced Manufacturing Technology*, vol. 41, no. 3-4, pp. 301–310, 2009.

[45] S. Ebeid and T. Ei-Taweel, "Surface improvement through hybridization of electrochemical turning and roller burnishing based on the taguchi technique," *Proceedings of the Institution of Mechanical Engineers, Part B: Journal of Engineering Manufacture*, vol. 219, no. 5, pp. 423–430, 2005.

[46] P. S. Prevey, N. Jayaraman, and R. Ravindranath, "Fatigue life extension of steam turbine alloys using low plasticity burnishing (lpb)," in *Proceedings of the ASME Turbo Expo*, 2010.

[47] J. M. Rao, A. C. K. Reddy, and P. R. Rao, "Experimental investigation of the influence of burnishing tool passes on surface roughness and hardness of brass specimens," *Indian Journal of Science and Technology*, vol. 4, no. 9, pp. 1113–1118, 2011.

[48] A. M. Hassan, "The effects of ball-and roller-burnishing on the surface roughness and hardness of some non-ferrous metals," *Journal of materials processing technology*, vol. 72, no. 3, pp. 385–391, 1997.

[49] A. Sagbas, "Analysis and optimization of surface roughness in the ball burnishing process using response surface methodology and desirabilty function," *Advances in Engineering Software*, vol. 42, no. 11, pp. 992–998, 2011.

[50] B. Tadic, P. M. Todorovic, O. Luzanin, D. Miljanic, B. M. Jeremic, B. Bogdanovic, and D. Vukelic, "Using specially designed high-stiffness burnishing tool to achieve high-quality surface finish," *The International Journal of Advanced Manufacturing Technology*, vol. 67, no. 1-4, pp. 601–611, 2013.

[51] A. M. Hassan and A. M. Maqableh, "The effects of initial burnishing parameters on non-ferrous components," *Journal of Materials Processing Technology*, vol. 102, no. 1-3, pp. 115–121, 2000.

[52] U. Shirsat and B. Ahuja, "Parametric analysis of combined turning and ball burnishing process," 2004.

[53] P. Balland, L. Tabourot, F. Degre, and V. Moreau, "An investigation of the mechanics of roller burnishing through finite element simulation and experiments," *International Journal of Machine tools and manufacture*, vol. 65, pp. 29–36, 2013.

[54] W. B. Saï and K. Saï, "Finite element modeling of burnishing of aisi 1042 steel," *The International Journal of Advanced Manufacturing Technology*, vol. 25, no. 5-6, pp. 460–465, 2005.

[55] M. S. John, A. W. Wilson, A. P. Bhardwaj, A. Abraham, and B. Vinayagam, "An investigation of ball burnishing process on cnc lathe using finite element analysis," *Simulation Modelling Practice and Theory*, vol. 62, pp. 88–101, 2016.

[56] A. Drechsler, J. Kiese, and L. Wagner, "Effects of shot peening and roller-burnishing on fatigue performance of various titanium alloys," *Shot peening, Institute of Precision Mechanics, Warsaw, Poland*, pp. 145–152, 1999.

[57] R. Sadeler, M. Akbulut, and S. Atasoy, "Influence of mechanical (ball burnishing) surface treatment on fatigue behaviour of aisi 1045 steel," *Kovove Materialy*, vol. 51, no. 1, pp. 31–5, 2013.

[58] A. M. Hassan and A. S. Al-Bsharat, "Improvements in some properties of non-ferrous metals by the application of the ball-burnishing process," *Journal of Materials Processing Technology*, vol. 59, no. 3, pp. 250–256, 1996.

[59] G. Leverant, B. Langer, A. Yuen, and S. Hopkins, "Surface residual stresses, surface topography and the fatigue behavior of ti-6ai-4v," *Metallurgical Transactions A*, vol. 10, no. 2, pp. 251–257, 1979.

[60] P. S. Prevéy, N. Jayaraman, and R. Ravindranath, "Low plasticity burnishing (lpb) treatment to mitigate fod and corrosion fatigue damage in 17-4 ph stainless steel," tech. rep., LAMBDA RESEARCH CINCINNATI OH, 2003.

[61] G. D. Revankar, R. Shetty, S. S. Rao, and V. N. Gaitonde, "Analysis of surface roughness and hardness in ball burnishing of titanium alloy," *Measurement*, vol. 58, pp. 256–268, 2014.

[62] M. Bourebia, A. Bouri, H. Hamadache, S. Achouri, L. Laouar, A. Gharbi, O. Ghelloudj, and K. Bouhamla, "Study of the effect burnishing on superficial hardness and hardening of s355jr steel using experimental planning," *Energy Procedia*, vol. 157, pp. 568–577, 2019.

[63] A. M. Hassan and A. M. Momani, "Further improvements in some properties of shot peened components using the burnishing process," *International Journal of Machine Tools and Manufacture*, vol. 40, no. 12, pp. 1775–1786, 2000.

[64] E. K. S. Maawad, *Residual Stress Analysis and Fatigue Behavior of Mechanically Surface Treated Titanium Alloys:(vom Promotionsausschuss Der Technischen Universität Clausthal Im Jahr 2012 Als Dissertation Angenommene Arbeit)*. Helmholtz-Zentrum Geesthacht, 2013.

[65] X. Yuan, Y. Sun, L. Gao, and S. Jiang, "Effect of roller burnishing process parameters on the surface roughness and microhardness for ta2 alloy," *The International Journal of Advanced Manufacturing Technology*, vol. 85, no. 5-8, pp. 1373–1383, 2016.

[66] F. Gharbi, S. Sghaier, H. Hamdi, and T. Benameur, "Ductility improvement of aluminum 1050a rolled sheet by a newly designed ball burnishing tool device," *The International Journal of Advanced Manufacturing Technology*, vol. 60, no. 1-4, pp. 87–99, 2012.

[67] M. Salahshoor and Y. Guo, "Process mechanics in ball burnishing biomedical magnesium–calcium alloy," *The International Journal of Advanced Manufacturing Technology*, vol. 64, no. 1-4, pp. 133–144, 2013.

[68] M. S. John and B. Vinayagam, "Optimization of ball burnishing process on tool steel (t215cr12) in cnc machining centre using response surface methodology," *Arabian Journal for Science and Engineering*, vol. 36, no. 7, pp. 1407–1422, 2011.

[69] A. H. Volume, "19: Fatigue and fracture," *ASM International*, vol. 19, 1996.

[70] H. E. Boyer *et al.*, *Atlas of fatigue curves*. Asm International, 1985.

[71] J. Schijve, "Fatigue of structures and materials in the 20th century and the state of the art," *International journal of fatigue*, vol. 25, no. 8, pp. 679–702, 2003.

[72] H. Grover, S. Gordon, and L. Jackson, "Fatigue of metals and structures us government printing office," *Revised Edition, June*, 1960.

[73] T. H. Courtney, *Mechanical behavior of materials*. Waveland Press, 2005.

[74] O. Föppl, "Das drücken der oberfläche von bauteilen aus stahl," *Stahl und Eisen*, vol. 49, pp. 575–577, 1929.

[75] D. J. Hornbach, P. S. Prevey, and E. F. Loftus, "Application of low plasticity burnishing (lpb) to improve the fatigue performance of ti-6al-4v femoral hip stems," *Journal of ASTM International*, vol. 3, no. 5, pp. 1–10, 2006.

[76] R. Avilés, J. Albizuri, A. Rodríguez, and L. L. De Lacalle, "Influence of low-plasticity ball burnishing on the high-cycle fatigue strength of medium carbon aisi 1045 steel," *International journal of fatigue*, vol. 55, pp. 230–244, 2013.

[77] P. S. Prevéy and J. Cammett, "Low cost corrosion damage mitigation and improved fatigue performance of low plasticity burnished 7075-t6," *Journal of Materials Engineering and Performance*, vol. 10, no. 5, pp. 548–555, 2001.

[78] P. Prevéy, J. Telesman, T. Gabb, and P. Kantzos, "Fod resistance and fatigue crack arrest in low plasticity burnished in718," in *Proceedings of the 5th Nat. Turbine Eng. HCF Conference*, 2000.

[79] W. Z. Zhuang and G. R. Halford, "Investigation of residual stress relaxation under cyclic load," *International journal of fatigue*, vol. 23, pp. 31–37, 2001.

[80] N. Jayaraman, P. S. Prevéy, and M. Mahoney, "Fatigue life improvement of an aluminum alloy fsw with low plasticity burnishing," in *Proceedings 132nd TMS Annual Meeting, San Diego, CA*, Citeseer, 2003.

[81] P. Prevéy, D. Hornbach, P. Mason, and M. Mahoney, "Improving corrosion fatigue performance of aa2219 friction stir welds with low plasticity burnishing," in *Proceedings of 2002 International Surface Engineering Conference. Columbus*, Citeseer, 2002.

[82] S. Hassanifard, H. Reyhani, A. Nabavi-Kivi, and A. Varvani-Farahani, "An experimental study of rolled friction-stir-welded aluminum 6061-t6 joints subjected to static and fatigue loading conditions," *Journal of Materials Engineering and Performance*, vol. 29, no. 7, pp. 4493–4505, 2020.

[83] J. A. Travieso-Rodríguez, R. Jerez-Mesa, G. Gómez-Gras, J. Llumà-Fuentes, O. Casadesús-Farràs, and M. Madueño-Guerrero, "Hardening effect and fatigue behavior enhancement through ball burnishing on aisi 1038," *Journal of Materials Research and Technology*, vol. 8, no. 6, pp. 5639–5646, 2019.

[84] C. Seemikeri, P. Brahmankar, and S. Mahagaonkar, "Low plasticity burnishing: an innovative manufacturing method for biomedical applications," *Journal of manufacturing science and engineering*, vol. 130, no. 2, 2008.

[85] I. Hutchings and P. Shipway, *Tribology: friction and wear of engineering materials.* Butterworth-Heinemann, 2017.

[86] B. Bhushan, *Modern tribology handbook, two volume set.* CRC press, 2000.

[87] R. Rajasekariah and S. Vaidyanathan, "Increasing the wear-resistance of steel components by ball burnishing," *Wear*, vol. 34, no. 2, pp. 183–188, 1975.

[88] A. M. Hassan and S. Z. Al-Dhifi, "Improvement in the wear resistance of brass components by the ball burnishing process," *Journal of Materials Processing Technology*, vol. 96, no. 1-3, pp. 73–80, 1999.

[89] G. D. Revankar, R. Shetty, S. S. Rao, and V. N. Gaitonde, "Wear resistance enhancement of titanium alloy (ti–6al–4v) by ball burnishing process," *Journal of Materials Research and Technology*, vol. 6, no. 1, pp. 13–32, 2017.

[90] H. Yilmaz and R. Sadeler, "Impact wear behavior of ball burnished 316l stainless steel," *Surface and Coatings Technology*, vol. 363, pp. 369–378, 2019.

[91] Z.-y. Zhou, G.-l. Yu, Q.-y. Zheng, G.-z. Ma, S.-b. Ye, C. Ding, and Z.-y. Piao, "Wear behavior of 7075-aluminum after ultrasonic-assisted surface burnishing," *Journal of Manufacturing Processes*, vol. 51, pp. 1–9, 2020.

[92] X. Wu, N. Tao, Y. Hong, G. Liu, B. Xu, J. Lu, and K. Lu, "Strain-induced grain refinement of cobalt during surface mechanical attrition treatment," *Acta Materialia*, vol. 53, no. 3, pp. 681–691, 2005.

[93] Y. Zhang, E. Feng, W. Mo, Y. Lv, R. Ma, S. Ye, X. Wang, and P. Yu, "On the microstructures and fatigue behaviors of 316l stainless steel metal injection molded with gas-and water-atomized powders," *Metals*, vol. 8, no. 11, p. 893, 2018.

[94] A. Saboori, M. Toushekhah, A. Aversa, M. Lai, M. Lombardi, S. Biamino, and P. Fino, "Critical features in the microstructural analysis of aisi 316l produced by metal additive manufacturing," *Metallography, Microstructure, and Analysis*, vol. 9, no. 1, pp. 92–96, 2020.

[95] R.-b. Song, J.-y. Xiang, and D.-p. Hou, "Characteristics of mechanical properties and microstructure for 316l austenitic stainless steel," *Journal of iron and steel research, international*, vol. 18, no. 11, pp. 53–59, 2011.

[96] M. J. Rao, C. K. A. Reddy, and R. P. Rao, "The effect of roller burnishing on surface hardness and surface roughness on mild steel specimens," *International Journal of Applied Engineering Research*, vol. 1, no. 4, p. 777, 2010.

[97] H. Hamadache, L. Laouar, N. Zeghib, and K. Chaoui, "Characteristics of rb40 steel superficial layer under ball and roller burnishing," *Journal of Materials Processing Technology*, vol. 180, no. 1-3, pp. 130–136, 2006.

[98] S. Bagherifard, S. Slawik, I. Fernández-Pariente, C. Pauly, F. Mücklich, and M. Guagliano, "Nanoscale surface modification of aisi 316l stainless steel by severe shot peening," *Materials & Design*, vol. 102, pp. 68–77, 2016.

[99] P. Sathiyamoorthi, J. Basu, S. Kashyap, K. Pradeep, and R. S. Kottada, "Thermal stability and grain boundary strengthening in ultrafine-grained cocrfeni high entropy alloy composite," *Materials & Design*, vol. 134, pp. 426–433, 2017.

[100] A. Bougharriou, W. B. Saï, and K. Saï, "Prediction of surface characteristics obtained by burnishing," *The International Journal of Advanced Manufacturing Technology*, vol. 51, no. 1-4, pp. 205–215, 2010.

[101] N. El-Tayeb, K. Low, and P. Brevern, "On the surface and tribological characteristics of burnished cylindrical al-6061," *Tribology International*, vol. 42, no. 2, pp. 320–326, 2009.

[102] F. Gharbi, S. Sghaier, F. Morel, and T. Benameur, "Experimental investigation of the effect of burnishing force on service properties of aisi 1010 steel plates," *Journal of Materials Engineering and Performance*, vol. 24, no. 2, pp. 721–725, 2015.

[103] P. Zhang and J. Lindemann, "Effect of roller burnishing on the high cycle fatigue performance of the high-strength wrought magnesium alloy az80," *Scripta materialia*, vol. 52, no. 10, pp. 1011–1015, 2005.

[104] A. Kumagai, T. D. Topping, *et al.*, *High cycle fatigue (HCF) testing of steel for Federal Aviation Administration (FAA) part qualification*. PhD thesis, 2017.

[105] P. S. Prevéy and J. T. Cammett, "The influence of surface enhancement by low plasticity burnishing on the corrosion fatigue performance of aa7075-t6," *International Journal of Fatigue*, vol. 26, no. 9, pp. 975–982, 2004.

[106] A. Aviles, R. Aviles, J. Albizuri, L. Pallares-Santasmartas, and A. Rodriguez, "Effect of shot-peening and low-plasticity burnishing on the high-cycle fatigue strength of din 34crnimo6 alloy steel," *International Journal of Fatigue*, vol. 119, pp. 338–354, 2019.

[107] T. Klotz, D. Delbergue, P. Bocher, M. Lévesque, and M. Brochu, "Surface characteristics and fatigue behavior of shot peened inconel 718," *International Journal of Fatigue*, vol. 110, pp. 10–21, 2018.

[108] J.-C. Kim, S.-K. Cheong, and H. Noguchi, "Residual stress relaxation and low- and high-cycle fatigue behavior of shot-peened medium-carbon steel," *International Journal of Fatigue*, vol. 56, pp. 114–122, 2013.

[109] R. Eslami, H. Riesch-Oppermann, and O. Kraft, "Prediction of multiaxial high cycle fatigue at small scales based on a micro-mechanical model," *International Journal of Fatigue*, vol. 83, pp. 66–74, 2016.

[110] S. Nelson, L. Ladani, T. Topping, and E. Lavernia, "Fatigue and monotonic loading crack nucleation and propagation in bimodal grain size aluminum alloy," *Acta Materialia*, vol. 59, no. 9, pp. 3550–3570, 2011.

[111] Y. Fu, N. L. Loh, A. W. Batchelor, D. Liu, X. Zhu, J. He, and K. Xu, "Improvement in fretting wear and fatigue resistance of ti–6al–4v by application of several surface treatments and coatings," *Surface and Coatings Technology*, vol. 106, no. 2-3, pp. 193–197, 1998.

[112] J. Del Abra-Arzola, M. García-Rentería, V. Cruz-Hernández, J. García-Guerra, V. Martínez-Landeros, L. Falcón-Franco, and F. Curiel-López, "Study of the

effect of sigma phase precipitation on the sliding wear and corrosion behaviour of duplex stainless steel aisi 2205," *Wear*, vol. 400, pp. 43–51, 2018.

[113] W. Liang, X. Bin, Y. Zhiwei, and S. Yaqin, "The wear and corrosion properties of stainless steel nitrided by low-pressure plasma-arc source ion nitriding at low temperatures," *Surface and Coatings Technology*, vol. 130, no. 2-3, pp. 304–308, 2000.

[114] B. Denkena and A. Lucas, "Biocompatible magnesium alloys as absorbable implant materials–adjusted surface and subsurface properties by machining processes," *CIRP annals*, vol. 56, no. 1, pp. 113–116, 2007.

[115] M. Torres and H. Voorwald, "An evaluation of shot peening, residual stress and stress relaxation on the fatigue life of aisi 4340 steel," *International Journal of Fatigue*, vol. 24, no. 8, pp. 877–886, 2002.

[116] G. Farrahi, J. Lebrijn, and D. Couratin, "Effect of shot peening on residual stress and fatigue life of a spring steel," *Fatigue & Fracture of Engineering Materials & Structures*, vol. 18, no. 2, pp. 211–220, 1995.

[117] C. A. V. Jiménez, G. G. Rosas, C. R. González, V. G. Alejo, and S. Hereñú, "Effect of laser shock processing on fatigue life of 2205 duplex stainless steel notched specimens," *Optics & Laser Technology*, vol. 97, pp. 308–315, 2017.

[118] K. Bettahar, M. Bouabdallah, R. Badji, M. Gaceb, C. Kahloun, and B. Bacroix, "Microstructure and mechanical behavior in dissimilar 13cr/2205 stainless steel welded pipes," *Materials & Design*, vol. 85, pp. 221–229, 2015.

[119] A. Hassan, "An investigation into the surface characteristics of burnished cast al cu alloys," *International Journal of Machine Tools and Manufacture*, vol. 37, no. 6, pp. 813–821, 1997.

[120] Y. Sun and T. Bell, "Sliding wear characteristics of low temperature plasma nitrided 316 austenitic stainless steel," *Wear*, vol. 218, no. 1, pp. 34–42, 1998.

[121] M. Peruzzo, F. Serafini, M. Ordoñez, R. Souza, and M. Farias, "Reciprocating sliding wear of the sintered 316l stainless steel with boron additions," *Wear*, vol. 422, pp. 108–118, 2019.

[122] Y. Sun, A. Moroz, and K. Alrbaey, "Sliding wear characteristics and corrosion behaviour of selective laser melted 316l stainless steel," *Journal of materials engineering and performance*, vol. 23, no. 2, pp. 518–526, 2014.

[123] B. Hashemi, M. R. Yazdi, and V. Azar, "The wear and corrosion resistance of shot peened–nitrided 316l austenitic stainless steel," *Materials & Design*, vol. 32, no. 6, pp. 3287–3292, 2011.

[124] D. E. Knuth, *The TEX Book*. Reading, Massachusetts: Addison-Wesley, 1984. Reprinted as Vol. A of *Computers & Typesetting*, 1986.

[125] J. Scheel, P. Prevéy, and D. Hornbach, "Prevention of corrosion related failure of aircraft aluminum using an engineered residual stress field," in *DoD Corrosion Conference, La Quinta, USA*, vol. 31.

[126] D. E. Knuth, *TEX: The Program*, vol. B of *Computers & Typesetting*. Reading, Massachusetts: Addison-Wesley, 1986.

[127] N. E. Nanninga, "High cycle fatigue of aa6082 and aa6063 aluminum extrusions," 2008.

[128] A. F. Padilha, R. L. Plaut, and P. R. Rios, "Stainless steel heat treatment," in *Steel Heat Treatment*, pp. 706–751, CRC Press, 2006.

[129] D. M. Escriba, E. Materna-Morris, R. L. Plaut, and A. F. Padilha, "Chi-phase precipitation in a duplex stainless steel," *Materials Characterization*, vol. 60, no. 11, pp. 1214–1219, 2009.

[130] C. V. Cooper and C. J. Isabelle, "Broad-beam ion deposition coating methods for depositing diamond-like-carbon coatings on dynamic surfaces," Jan. 9 1996. US Patent 5,482,602.

[131] D. E. Knuth, "The WEB system for structured documentation, version 2.3," Tech. Rep. STAN-CS-83-980, Computer Science Department, Stanford University, Stanford, California, Sept. 1983.

[132] D. E. Knuth, "Literate programming," *The Computer Journal*, vol. 27, pp. 97–111, May 1984.

[133] J. Fleming and N. Suh, "Mechanics of crack propagation in delamination wear," *Wear*, vol. 44, no. 1, pp. 39–56, 1977.

[134] D. E. Knuth, "A torture test for TEX, version 1.3," Tech. Rep. STAN-CS-84-1027, Computer Science Department, Stanford University, Stanford, California, Nov. 1984.

[135] R. K. Furuta and P. A. MacKay, "Two TEX implementations for the IBM PC," *Dr. Dobb's Journal*, vol. 10, pp. 80–91, Sept. 1985.

[136] J. Désarménien, "How to run TEX in french," Tech. Rep. SATN-CS-1013, Computer Science Department, Stanford University, Stanford, California, Aug. 1984.

[137] A. L. Samuel, "First grade TEX: A beginner's TEX manual," Tech. Rep. SATN-CS-83-985, Computer Science Department, Stanford University, Stanford, California, Nov. 1983.

[138] L. Lamport, *LATEX: A Document Preparation System. User's Guide and Reference Manual.* Reading, Massachusetts: Addison-Wesley, 1986.

[139] M. D. Spivak, *The Joy of TEX.* American Mathematical Society, 1985.

[140] O. Patashnik, *BibTEXing*. Computer Science Department, Stanford University, Stanford, California, Jan. 1988. Available in the BibTEX release.

[141] O. Patashnik, *Designing BibTEX Styles*. Computer Science Department, Stanford University, Jan. 1988.

[142] D. Fuchs, "The format of TEX's DVI files version 1," *TUGboat*, vol. 2, pp. 12–16, July 1981.

[143] D. Fuchs, "Device independent file format," *TUGboat*, vol. 3, pp. 14–19, Oct. 1982.

[144] H. Hertz, "About the contact of elastic solid bodies (über die berührung fester elastischer körper)," *J Reine Angew Math*, vol. 5, pp. 12–23, 1881.